



Field study on post-grouting effects of cast-in-place bored piles in extra-thick fine sand layers

Zhi-hui Wan¹ · Guo-liang Dai¹ · Wei-ming Gong¹

Received: 3 October 2017 / Accepted: 9 October 2018 / Published online: 16 October 2018
© Springer-Verlag GmbH Germany, part of Springer Nature 2018

Abstract

The post-pressure grouting technique has proven to be an effective method to enhance axial resistance. In this paper, field tests were conducted to investigate the performances of large-diameter cast-in-place bored piles for six combined side-and-tip grouting piles and two side-grouting piles in extra-thick fine sand layers. The load–displacement response, shaft resistance, and mobilization of unit base resistance were discussed. The field results indicate that compared with the piles before post-grouting both the shaft resistance and base resistance for the piles after post-grouting are significantly improved. The piles after post-grouting have higher load-bearing capacity. Meanwhile, the load-bearing capacity of combined-grouting piles is also greater than that of side-grouting piles. Additionally, the strengthening effect of the surrounding soil improvement due to side grouting on the base resistance can enhance the unit base resistance, and the unit shaft resistance can also be increased by the soil improvement at the pile tip due to tip grouting. Moreover, the distribution of the injected pressurized grout at the pile tip and side is detected by an electromagnetic wave computerized tomography (EWCT) technique. The results reveal that EWCT can detect the distribution pattern of the pile, injected grout and geotechnical interface and evaluate the diffusion range of the grout of the soil at the pile tip and side, which can be used to assess the grouting effect of grouted piles. Finally, an in situ standard penetration test is employed to evaluate the grouting effect of grouted pile by variation of the SPT N value before and after post-grouting. The research results have reference value and guiding significance for the design and effect detection of post-grouting piles.

Keywords Cast-in-place bored pile · Combined post-grouting at pile tip and side · Electromagnetic wave computerized tomography · Extra-thick fine sand layer · Post-grouting at pile side · Standard penetration test

1 Introduction

With the constant emergence of high-rise buildings, long-span bridges, high-speed railways, and marine engineering, cast-in-place bored piles have gained widespread application because of their high bearing capacity, flexibility, and adaptability. However, soil disturbances beneath the pile

tip due to the drilling process, which has great influence on the tip resistance, and debris remaining after cleanout will further reduce the tip resistance [7, 24, 26, 27, 40]. Meanwhile, the soil stress surrounding the pile during the drilling process is released, which will also reduce the shaft resistance [9, 22, 25, 44]. Additionally, the mobilization of the tip resistance is hampered by the softening of the pile tip condition. It can thus be seen that the application of bored piles is significantly affected by these issues. Accordingly, the post-grouting technique is considered to be an effective means to mitigate the abovementioned issues and improve the bearing performance of cast-in-place bored piles. The cement grout is injected into the soil at the pile tip and side, and the strength and stiffness of the soil at the pile tip and side are enhanced by means of permeating, compacting, and splitting, thereby improving the axial capacity and reducing the pile settlement.

✉ Guo-liang Dai
daigl@seu.edu.cn; seudaigl@126.com

Zhi-hui Wan
seuwanzhahui@163.com

Wei-ming Gong
wmgong@seu.edu.cn

¹ Key Laboratory of Concrete and Prestressed Concrete Structures of Ministry of Education, School of Civil Engineering, Southeast University, Nanjing 211189, China

Therefore, the post-grouting technique has recently been applied to many engineering projects, especially major engineering projects, and achieved significant economic and social benefits.

Post-grouting at the pile tip has been successfully employed throughout the world for the past six decades and has proven to be an effective method to improve axial resistance and reduce settlement [1, 2, 6, 23, 26, 36, 37]. Alternately, the application of post-grouting at the pile side is slightly more recent than post-grouting at the pile tip, and there is little reported in the literature. Gouvenot and Gabaix [11] first published that the shaft grouting was applied to the steel piles, and full-scale load tests were conducted in three shaft grouted piles in sand and three shaft grouted piles in clay; the results indicated that the bearing capacity of the grouted steel piles was 2.5 times higher than that of the ungrouted steel piles under the same conditions. Littlechild et al. [18] reported that static load tests were carried out on 20 side-grouting piles up to 1.5 m in diameter in sand and clay with SPT N values less than 50, and the conclusion of the tests was that the shaft resistance of side-grouting piles was double that of ungrouted piles. Moreover, reloading tests over a year after the first load test were performed on the side-grouting piles, and the shaft resistance of the side-grouting piles was not reduced. Consequently, post-grouting at the pile side can effectively improve the boundary conditions at the pile-soil contact and strengthen the strength and stiffness of the soil around the pile shaft, thereby increasing the shaft resistance [3, 19, 21, 28]. In practice, large-diameter bored piles are usually installed in the soil to resist greater vertical, lateral, and uplift loads and have been widely applied in the foundation of highway bridges, high-voltage transmission towers, underground substations and offshore oil platforms. However, the pile shaft in the abovementioned foundation is often affected by the combined actions of axial force, horizontal shear and moment, whereas it may be difficult to meet the pile foundation design requirements with tip grouting alone. Therefore, it is necessary to use side grouting or combined tip-and-side grouting to further improve the bearing capacity of large-diameter bored piles. On this basis, there is a need to analyze the response of side-grouting piles and combined-grouting piles.

Post-grouting craftwork is underground concealed engineering and its effect can be affected by the uncertainty of the grouting process and the complexity of the influencing factors; the evaluation of the grouting effect is thus more difficult. At present, the detection methods of the grouting effect include the static load test, coring test, and standard penetration test [5, 13, 17]. The static load test is the most direct and effective method for determining the bearing capacity of the pile foundation before and after post-grouting and can analyze the grouting effect

quantitatively. However, this method can only determine the representative part of the pile and is not suitable for mass production piles. The distribution of cement grout along the pile length and physical and mechanical properties of cement–soil coring samples after post-grouting can be detected by the coring test. However, the penetration direction of cement grout and the quantity of cement are uncertain due to the anisotropy and inhomogeneity of the soil, causing the test results to have great limitations. The standard penetration test is a more intuitive and accurate detection method, but only the vertical variation of the formation in one borehole can be found. The cost and period of the test may be multiplied if a large number of boreholes are arranged to understand the characteristics of the horizontal variation of the formation. Therefore, it is necessary to study a nondestructive method for rapid, effective and practical grouting effect.

In this paper, the field tests are carried out on eight large-diameter cast-in-place bored piles in extra-thick fine sand layers, including six combined side-and-tip grouting piles and two side-grouting piles. The load–displacement response, shaft resistance, and base resistance under axial load in extra-thick fine sand layers are estimated from the strain gauge data obtained during the bi-directional O-cell tests, and the results of combined-grouting piles and side-grouting piles before and after post-grouting are compared and analyzed. Furthermore, the reinforcement effect of combined tip-and-side grouting is detected by an electromagnetic wave computerized tomography technique to investigate the effect of the post-grouting technique in the application of large bridge pile foundations. Finally, an in situ standard penetration test is employed to evaluate the grouting effect of grouted piles by the variation of SPT N values before and after post-grouting. It is expected to provide a basis for the design and detection of post-grouting piles.

2 Review of the post-grouting apparatus at the pile tip and side

The post-grouting technique was first applied to the construction of Maracaibo Bridge pile foundations in 1958, and the bearing capacity of the pile foundation was improved by the base grouting of the prefabricated pile. Since then, grouting techniques have been gradually applied in pile foundation engineering throughout the world and have been continuously innovated and developed. Bolognesi and Moretto [1] described in detail that the method of the pile base grouting via preloading cell apparatus has been employed for the bridge pile foundations on the Parana River, while a closed grouting device for the pressure chamber has also been developed by Lizzi

et al. [20]. Sliwinski and Fleming [27] introduced an open grouting device for *U*-shaped grouting cells, which was placed in gravel and has a rubber sleeves perforated steel pipe at the end of the pile. Bruce [2] reported that a simplified *U*-shaped grouting device, which was fixed to the steel reinforcement cage and placed at the pile base, was used in the construction of the pile foundation of a cable-stayed bridge in Thailand in 1985. Mullins and Dapp [7, 24] presented that the three grouting apparatuses at pile tip were flat jack (similar to that discussed by Lizzi et al.), sleeve-port (similar to that described by Bruce), and sleeve-port with steel plate (similar to that introduced by Sliwinski and Fleming), respectively. In addition, the flat jack, *U*-shaped and modified *U*-shaped apparatuses for the base sediment treatment were introduced by Lin et al. [17], while Thasnanipan et al. [31] described the two different base grouting devices, known as tube-*à*-manchette and drill-and-grout, commonly applied in Bangkok.

In practice, the application of post-grouting at the pile side is slightly more recent than post-grouting at the pile tip. Gouvenot and Gabaix [11] proposed first that a shaft grouting device, which was placed in a 508-mm-in-diameter steel pile, and an injection point was arranged at intervals of 1 m along the grouting pipes. A shaft grouting model test apparatus for driven piles in calcareous sand was developed by Joer et al. [15]; this apparatus comprised a grouting pump and grouting tubes, in which the grouting tubes were fixed on the inside of the pile and injected grout into the sidewall to achieve the anticipated grouting pressure and grouting volume through the valve to control the grouting process. Fu and Zhou [10] introduced a sleeve valve pipe device for side-grouting, which involved grouting tubes, pressure transfer tubes and stopping-grout valve, and applied it to improve the axial resistance of bored piles. More recently, Sze and Chan [29] described how the shaft grouting apparatus was applied in the barrette pile and underground diaphragm wall of a building project in Hong Kong. The apparatus adopted for shaft grouting consisted of 50-mm-in-diameter mild steel tubes, with rubber sleeves spaced at intervals of 1 m along the grouting tubes. A new jetted and grouted precast pile containing separate devices for side-and-tip grouting was designed by Thiyyakkandi et al. [35, 37]; the side-grouting system was divided into different grouting zones according to the pile length, and each has an independent pipe network. Each of the side-grouting tubes has an entry and an exit outlet, and the tip half of each grouting tube has a series of holes at spacings of 127 mm, with rubber sleeves covering the holes. To prevent cement grout from moving along the weakest path during side-grouting, membranes are mounted to the precast pile. Additionally, Zhou et al. [46, 47] reported a pre-bored grouting planted pile system, which was grouted along the pile hole after the drilling was

completed and put the precast pile into the pile hole through its own weight after the end of grouting.

The post-grouting technique was first applied in China to strengthen the gravel stratum at the pile tip in the 1980s. Since then, the grouting technique has gained widespread development and application in the territory. The post-grouting technique, from the development of closed grouting to open grouting, from post-grouting at the pile tip to post-grouting at the pile side or tip-and-side, from the single pipe method to the *U*-shaped pipe method, has now developed into a more mature construction craftwork. In China, tip grouting apparatuses are generally divided into two broad categories: the single pipe method, or the *U*-shaped pipe method. The single pipe method usually consists of grouting pipes with rubber sleeves wrapped underneath, as shown in Fig. 1a. The *U*-shaped pipe method typically consists of one grouting pipe, one return pipe and one tip-manchette, as shown in Fig. 1b. A detailed description of grouting apparatuses at the pile tip can be found in the literature [9, 38]. Similarly, side-grouting apparatuses are generally divided into two broad categories: the single pipe method set to grouting pipes along the longitudinal direction of the steel rebar cage, or the ring pipe method set to grouting pipes along the circumferential direction of the steel rebar cage. The single pipe method for side grouting generally includes the grouting pipes, elbows and side-manchette, as shown in Fig. 2a. The grouting pipes, which are fixed to the inside of the steel rebar cage using normal tie wire, are used as the grout delivery system. The side-manchette, which is fixed to the outside of the steel rebar cage, is connected to the bottom of the grouting pipe by an elbow, and the side-manchette is similar to the tip-manchette of the single pipe method for tip grouting. Meanwhile, the number of grouting pipes, which can be properly adjusted according to the pile diameter, is not generally less than four along the steel rebar cage. The ring pipe method for side grouting entails one grouting pipe, one tee joint and one side-manchette, as shown in Fig. 2b. The side-manchette, which is a reinforced flexible hose that surrounds the outside of the steel rebar cage, is connected to the grouting pipe set to the inside of the steel rebar cage by a tee joint. The reinforced flexible hose can be circumferentially arranged with 4–6 rows of grout holes according to the pile diameter, and the grout holes are wrapped with rubber sleeves in rows to act as one-way valves. The number of cross sections of grouting pipes for side grouting depends on the pile length, and the location of cross sections of grouting pipes at the pile side can be determined according to the Chinese standards JTJD63-2007 and JGJ94-2008 [32, 33] and the geological prospecting data. Generally, the first cross section of the grouting pipes at the pile side is located at the

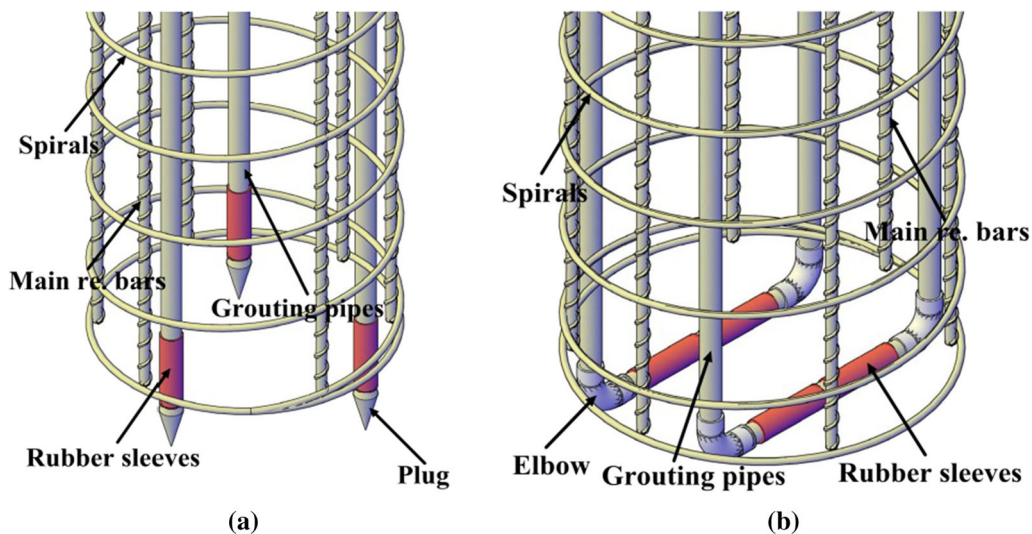


Fig. 1 The grouting apparatus at the pile tip: **a** single pipe method; **b** U-shaped pipe method

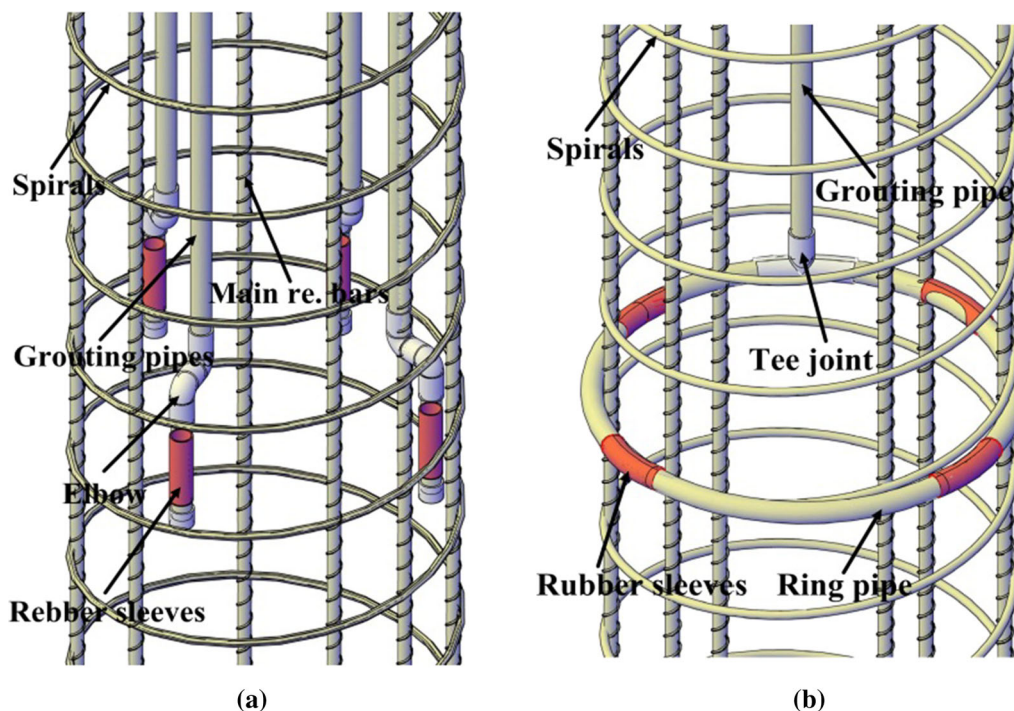


Fig. 2 The grouting apparatus at the pile side: **a** the single pipe method set to grouting pipes along the longitudinal direction of the steel rebar cage; **b** the ring pipe method set to grouting pipes along the circumferential direction of the steel rebar cage

position of 8–15 m above the pile tip and then arranged upward one by one along the pile length.

3 Background

Shishou Yangtze River Highway Bridge is located in Shishou, Hubei Province, Central China. The total length of the proposed bridge is approximately 39.7 km, of which

the lengths of the main bridge and approach bridges are 1.45 km and 8.08 km, respectively. The proposed bridge, which is a large-scale project with high technical content, is a world-class bridge project. Figure 3 shows a sectional view of the main bridge. Large-diameter cast-in-place bored pile foundations were employed in the main and approach bridges, with a total of two hundred and ninety-nine piers installed along the main and approach bridges. The results of geological drilling along the proposed bridge

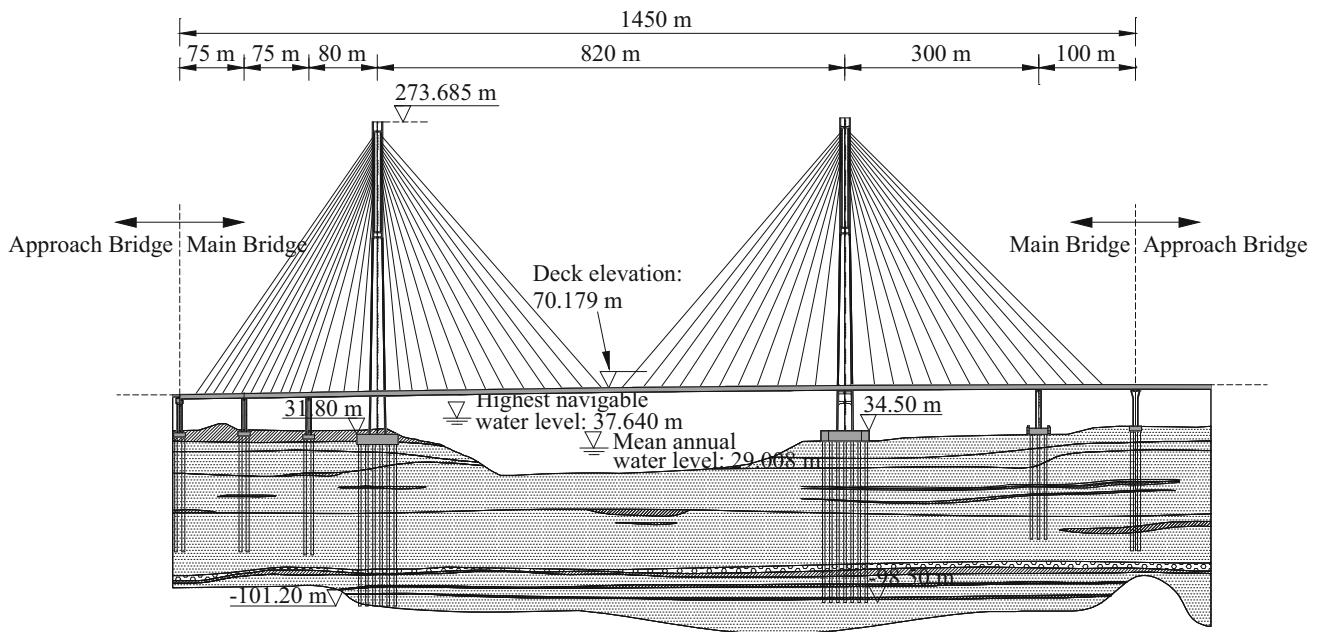


Fig. 3 Layout of the main bridge

site show that there is no bedrock in the exploration of 180 m, and the regional geological conditions are relatively simple and mainly composed of a fine sand layer. To understand the behavior of large-diameter cast-in-place bored piles in the extra-thick fine sand layer, it is necessary to carry out test piles at the proposed bridge site.

4 Site description

Sufficient boreholes were sunk to obtain detailed distributions of the soil layers, and in situ standard penetration tests (SPT) and cone penetration tests (CPT) were performed prior to the design of pile foundations. Four CPT boreholes (BR1, BR2, BR3, and BR4) and four SPT boreholes (BH1, BH2, BH3, and BH4) were carried out near the test piles of the north and south approach bridges; the locations of the

site investigation are illustrated in Fig. 4. The groundwater table at the proposed bridge site was encountered at depths between 1.5 and 2.0 m. The detailed soil layer distributions at the proposed bridge site are shown in Fig. 5. As shown in Fig. 5, the soil layer at the site is composed of mucky soil, clay, silty clay, silt and fine sand. Table 1 summarizes the soil profiles and properties for each soil layer of the north and south approach bridges.

Figure 6 shows the results of the CPT sounding at boreholes BR1, BR2, BR3, and BR4. The soundings were terminated below approximately 22 m in depth because of the strength of medium dense fine sand. The SPT blow-count (N) with the depth near the test piles is also shown in Fig. 5. Figure 5 shows that the SPT N values of the cohesive soil at the shallow layer vary between 2 and 11, whereas the SPT N values of the fine sand soil at the deep

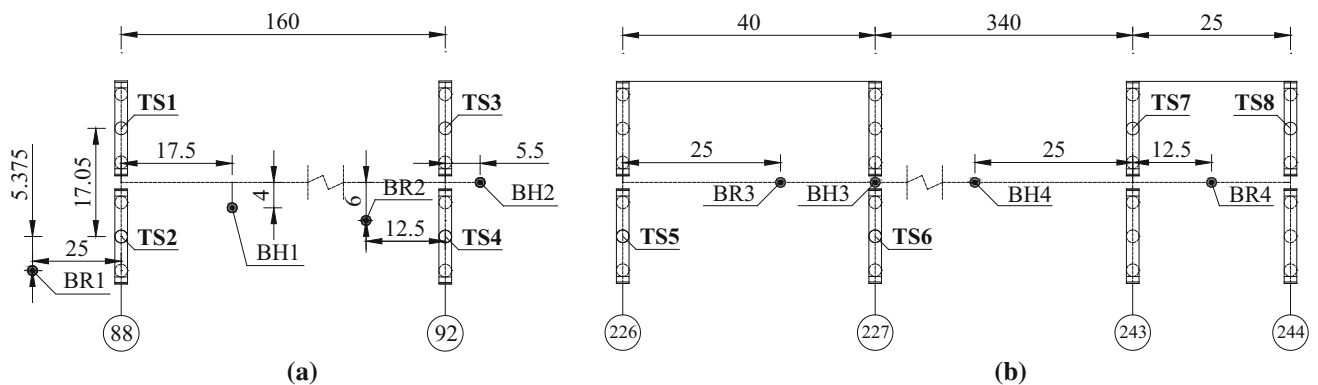


Fig. 4 The locations of SPT and CPT data near a test piles of the north approach bridge and b test piles of the south approach bridge (unit: m)

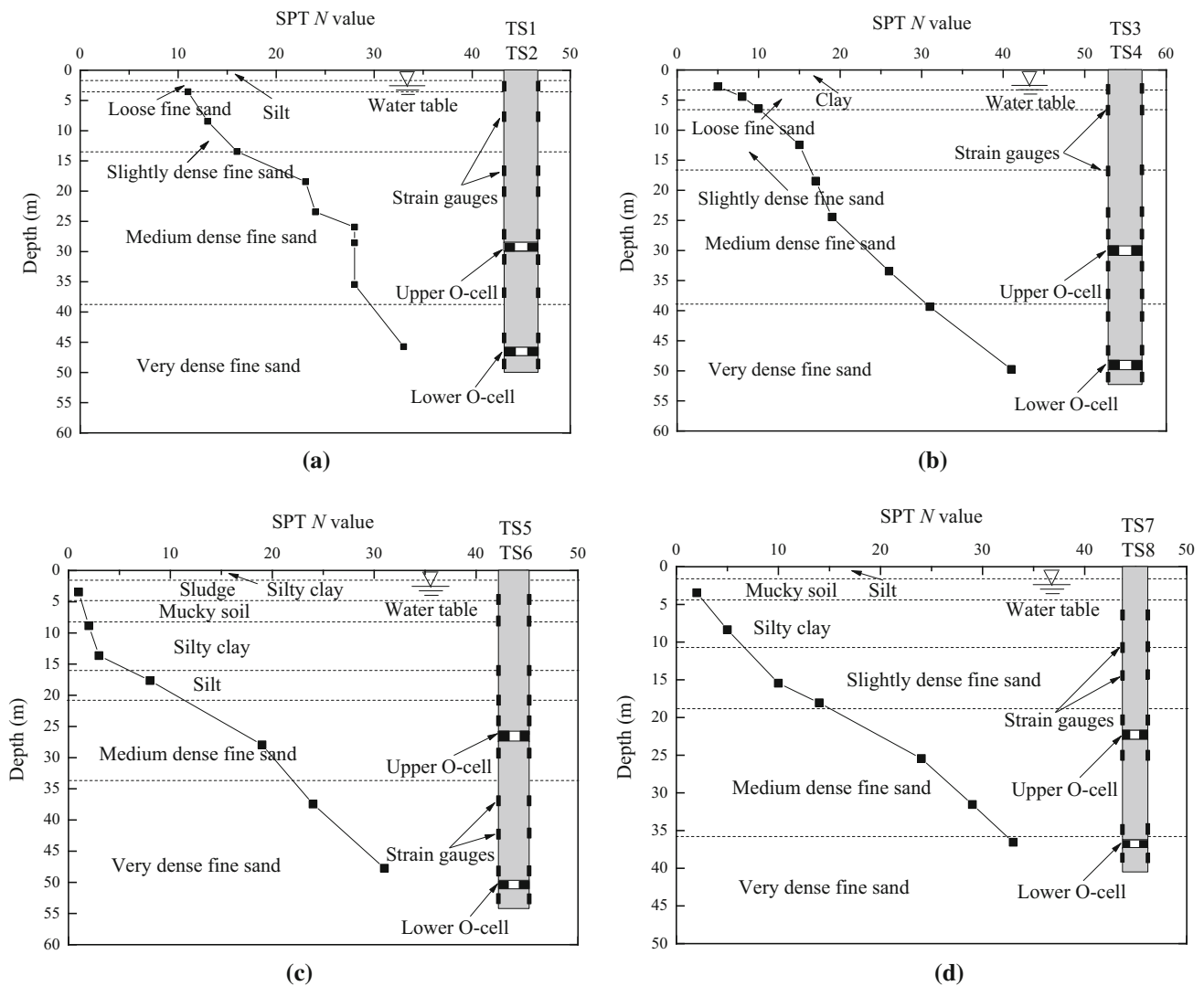


Fig. 5 Typical soil profiles, SPT N variations, and shaft instrumentation: **a** borehole BH1 near piles TS1 and TS2; **b** borehole BH2 near piles TS3 and TS4; **c** borehole BH3 near piles TS5 and TS6; and **d** borehole BH4 near piles TS7 and TS8

layer vary between 16 and 41; the fine sand soils at the deep layer are in a medium dense to very dense state.

5 Test pile conditions, test method, and instrumentation

Eight large-diameter cast-in-place bored piles in the extra-thick fine sand layer were tested to study the response of an axially loaded single pile. The test piles TS1, TS2 and the test piles TS3, TS4 are located on pier no. 88 and pier no. 92 of the north approach bridge, respectively; the test piles TS5 and TS6 are located on pier no. 226 and pier no. 227 of the south approach bridge, respectively, whereas the test piles TS7 and TS8 are located on pier no. 243 and pier no. 244 of the south approach bridge, respectively. The layout of the eight test piles is shown in Fig. 4, and the soil

profiles of the location of each test pile in the soil layers are shown in Fig. 5. The test piles of the north approach bridge were installed using the reverse circulation rotary drilling method, and the other test piles of the south approach bridge were installed using the auger drilling method. The elastic modulus of the concrete for each test pile was assumed to be 30 GPa. All the test piles rested on a layer of very dense fine sand, and the other detailed parameters of the test piles are shown in Table 2.

The static load tests were conducted in two phases: before and after post-grouting. The first phase was commenced after the concrete reached the design strength of the pile shaft. The second phase was conducted after post-grouting and the requirements of the grout curing were met.

The bi-directional O-cell test method was employed in the field tests of the test piles, and a double-level O-cell is placed in the shafts for this test. The positions of the

Table 1 Soil parameters

Soil layer	w (%)	γ_{sat} (kN m ⁻³)	e	E_{s1-2} (MPa)	c (kPa)	ϕ (°)	f_{sa} (kPa)	q_{sik} (kPa)
<i>North approach bridge</i>								
Clay	31.5	18.9	0.901	4.43	16.2	13.9	100	40.8
Silt	31.1	18.9	0.881	4.30	14.7	13.8	100	23.3
Loose fine sand	20.6	19.0	0.968	8.6	15.3	27.74		
Slightly dense fine sand		19.7	0.892	10.2	16.0	30.7	140	33.7
Medium dense fine sand		20.2	0.808	12.0	15.0	33.0	190	49.6
Very dense fine sand		20.5	0.672	12.4	15.0	33.9		
<i>South approach bridge</i>								
Sludge	64.1	16.3	1.776	2.18	4.8	4.1	50	22.7
Mucky soil	45.1	17.7	1.251	2.72	6.5	5.6	80	31.9
Silty clay	37.3	18.3	1.045	3.44	11.2	7.1	100	40.8
Silt	26.6	19.3	0.772	9.60	24.2	20.0	130	48.2
Slightly dense fine sand		19.7	0.892	10.2	16.0	30.7	140	33.7
Medium dense fine sand		20.2	0.808	12.0	15.0	33.0	190	49.6
Very dense fine sand		20.5	0.672	12.4	15.0	33.9		

w , the natural water content; γ_{sat} , the saturated unit weight; e , the void ratio; E_{s1-2} , the compressive modulus; c and ϕ , the cohesion and internal friction angle of each soil layer, respectively; f_{sa} , the characteristic value of the strata bearing capacity; and q_{sik} , the standard value of shaft resistance, estimated from cone penetration tests

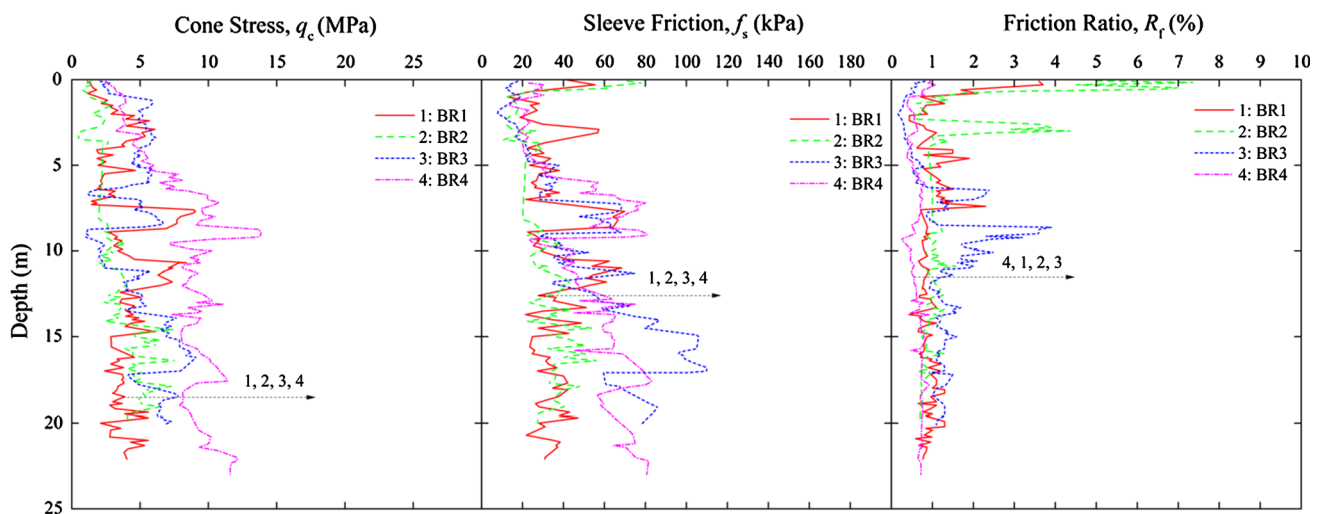


Fig. 6 Cone penetration test results at boreholes (BR1, BR2, BR3, and BR4)

double-level O-cell for the test piles are presented in Fig. 5. The bi-directional O-cell tests were conducted on the test piles in accordance with the slowly maintained load procedure. The methods of loading and unloading were in accordance with the Chinese standard JGJ/T 403-2017 [34]. A detailed description of the double-level O-cell test was provided by Wan et al. [39]. To investigate the influence of post-grouting on the bearing characteristics of large-diameter cast-in-place bored piles, strain gauges were mounted to the reinforcing cage at each level before the installation of test piles. Figure 5 presents the elevations of strain gauges along the test pile. Two displacement transducers were installed at the pile head to measure the pile

head displacement, and four displacement transducers were mounted at the upper and the lower level of the O-cell to measure the displacement of the upper and lower O-cell.

6 Post-grouting technique

After the test piles were formed, the post-grouting technique was adopted to enhance the axial resistance and reduce the settlement of the test piles. The test piles TS2, TS3, TS4, TS5, TS6, and TS8 were subjected to the combined tip-and-side grouting, and the test piles TS1 and TS7 were underwent post-grouting at the pile side alone.

Table 2 Parameters of test piles

Pile no.	Pile diameter (m)	Pile length (m)	Bearing stratum	Design load (kN)	Test phase
TS1	2.0	50	Fine sand	15,340	Before and after post-grouting
TS2	2.0	50	Fine sand	15,340	Before and after post-grouting
TS3	2.0	52	Fine sand	15,820	Before and after post-grouting
TS4	2.0	52	Fine sand	15,820	Before and after post-grouting
TS5	1.8	54	Fine sand	14,380	Before and after post-grouting
TS6	1.8	54	Fine sand	14,440	Before and after post-grouting
TS7	1.5	40	Fine sand	9842	Before and after post-grouting
TS8	1.5	40	Fine sand	9400	Before and after post-grouting

The design load is estimated synthetically by the standard penetration tests and the cone penetration tests

As previously described, the grouting device at the pile tip is post-grouted using the single pipe method, and three vertical tip-manchettes, each connected to the bottom of one grouting pipe, are installed at the bottom of the pile excavation with the steel rebar cage. The grouting device at the pile side is post-grouted using the ring pipe method set to grouting pipes along the circumferential direction of the steel rebar cage. For the test piles TS2, TS3, TS4, TS5, TS6, TS7, and TS8, two ring grouting pipes are placed along the steel rebar cage at two levels, while for the test pile TS1, three ring grouting pipes are placed along the steel rebar cage at three levels. The number and location of the grouting pipe at the pile tip and side are determined according to the Chinese standards JTJD63-2007 and JGJ94-2008 and geotechnical investigations. The position of grouting ring pipes above the pile tip for each pile is summarized in Table 3. The Chinese standard JGJ94-2008 states that, regarding the sequence of combined side-and-tip grouting, grouting at the pile side should first be performed, followed by grouting at the pile tip. Additionally, when pile side-grouting pipes were attached to the reinforcement cage of the test piles at different levels, the side grouting should be performed from pile head to pile bottom. It should be noted that the time interval of the side grouting and the tip grouting should not be less than 2 h. Photographs taken during the installation of the grouting device at the pile tip and side are given in Fig. 7.

To prevent the grouting pipes from experiencing blockage, after 12 h of pouring concrete, water is pumped through the grout delivery system to break off concrete from the tip-manchette or side-manchette. After the concrete has reached the design strength of the pile shaft, the first phase test of the test piles is carried out by the bi-direction O-cell test method. The post-grouting of each test pile is conducted immediately after the end of the first phase test. The test piles are post-grouted using a mixture of water and ordinary Portland cement. The water-cement ratio of the grout is approximately 0.5:1, and the other

detailed grouting parameters of the test piles are described in Table 3.

7 Analysis of load test results

7.1 Equivalent load–displacement responses

The bi-directional O-cell tests of the first phase were carried out approximately 20 days after pouring concrete, and the bi-directional O-cell tests of the second phase were conducted approximately 30 days after post-grouting. The test results of the bi-directional O-cell before and after post-grouting were equivalently converted into the load–displacement curves of the conventional static load test. Detailed equivalent conversion of the bi-directional O-cell test can be found in the literature [6].

Figure 8 shows the equivalent load–displacement responses of each test pile before and after post-grouting. In Fig. 8, it is shown that the equivalent load–displacement curves of the test piles before and after post-grouting have distinct plunging points, and the equivalent pile head load–displacement curves of the test piles after post-grouting are gentler than those of the test piles before post-grouting. Zhang et al. [43] and Wan et al. [40] proposed that the load corresponding to the plunging point of the pile can be regarded as the ultimate bearing capacity of a single pile. Hence, the ultimate bearing capacity of each pile is taken to be the load before reaching the maximum load, i.e., when the equivalent applied load at the pile TS1 head before post-grouting is loaded from 21.3 MN to 21.9 MN, the equivalent displacement at the pile head sharply increases. According to the abovementioned criterion, the ultimate bearing capacity of each pile before and after post-grouting can be obtained. The ultimate bearing capacity, total shaft resistance, base resistance of each pile, and their corresponding increased range are summarized in Table 4.

Table 3 Grouting parameters

Pile no.	Water–cement ratio	Quantity of cement (t)		Grouting pressure (MPa)		Position of side pipes above the pile tip (m) First, second, third	Grouting type
		Pile side	Pile tip	Pile side	Pile tip		
TS1	0.5	3.6	N/A	3.9	N/A	8, 23, 38	Side grouting
TS2	0.5	3.0	4.0	2.7	4.2	15, 30, N/A	Combined grouting
TS3	0.5	3.4	3.6	2.8	4.3	15, 30, N/A	Combined grouting
TS4	0.5	3.4	3.6	2.9	4.2	15, 30, N/A	Combined grouting
TS5	0.5	3.2	2.8	4.2	5.5	15, 30, N/A	Combined grouting
TS6	0.5	3.2	2.82	4.8	5.7	15, 30, N/A	Combined grouting
TS7	0.5	2.5	N/A	2.7	N/A	8, 23, N/A	Side grouting
TS8	0.5	2.4	2.4	3.1	3.5	12, 24, N/A	Combined grouting

Only the grouting pressure of the first cross section of the grouting pipe at the pile side is given

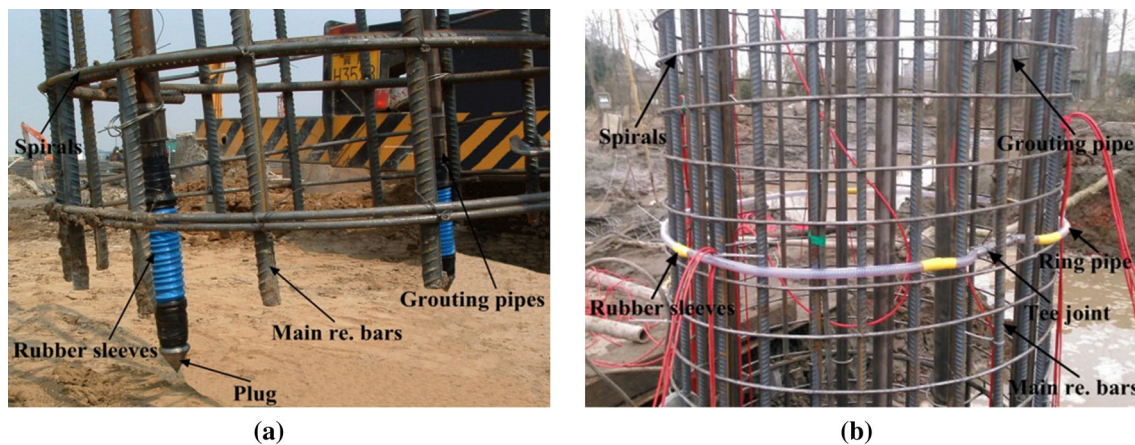


Fig. 7 The photographs of the site construction for tip-and-side post-grouting facilities: **a** grouting device at the pile tip; and **b** grouting device at the pile side

It can also be seen in Fig. 8 that the equivalent displacement of each pile head increases with increasing equivalent load of each pile head, and at a small loading level, the equivalent load–displacement curves for each pile before and after post-grouting are almost linear. The difference between the grouted piles and the ungrouted piles increases gradually with increasing equivalent load. The equivalent displacement increase at the pile head for grouted piles is less than that of ungrouted piles at the same load level. That is, the pile after post-grouting can bear greater pile head load at the same displacement. Consequently, under the same conditions, the bearing capacity of grouted piles is obviously larger than that of the piles without post-grouting. Meanwhile, the bearing capacity of combined-grouting piles is also greater than that of side-grouting piles.

The results in Table 4 show that compared with the test results of the piles TS1 and TS7 before side grouting, the ultimate bearing capacity of the piles TS1 and TS7 after

side grouting in the extra-thick fine sand layer is increased by 41.54% to 58.98%, the total shaft resistance is increased by 51.85% to 59.19%, and the base resistance is increased by 1.27% to 57.41%. In addition, the ultimate bearing capacity, the total shaft resistance and the base resistance of the piles TS2, TS3, TS4, TS5, TS6, and TS8 after combined tip-and-side grouting are 66.03–96.40%, 46.72–68.88%, and 137.87–323.01% larger than that before combined tip-and-side grouting, respectively. It can also be noted from the test results of the piles TS2, TS3, TS4, TS5, TS6, and TS8 after combined tip-and-side grouting that the ratios of the base resistance to the ultimate bearing capacity for the piles TS2, TS3, TS4, TS5, TS6, and TS8 are increased from 10.83–21.16% to 22.25–30.32%, and the pile functions are thereby converted into an end-bearing friction pile. Therefore, the bearing performance of the combined-grouting pile is better than that of the side-grouting pile, and the load transfer characteristics of the pile are significantly improved.

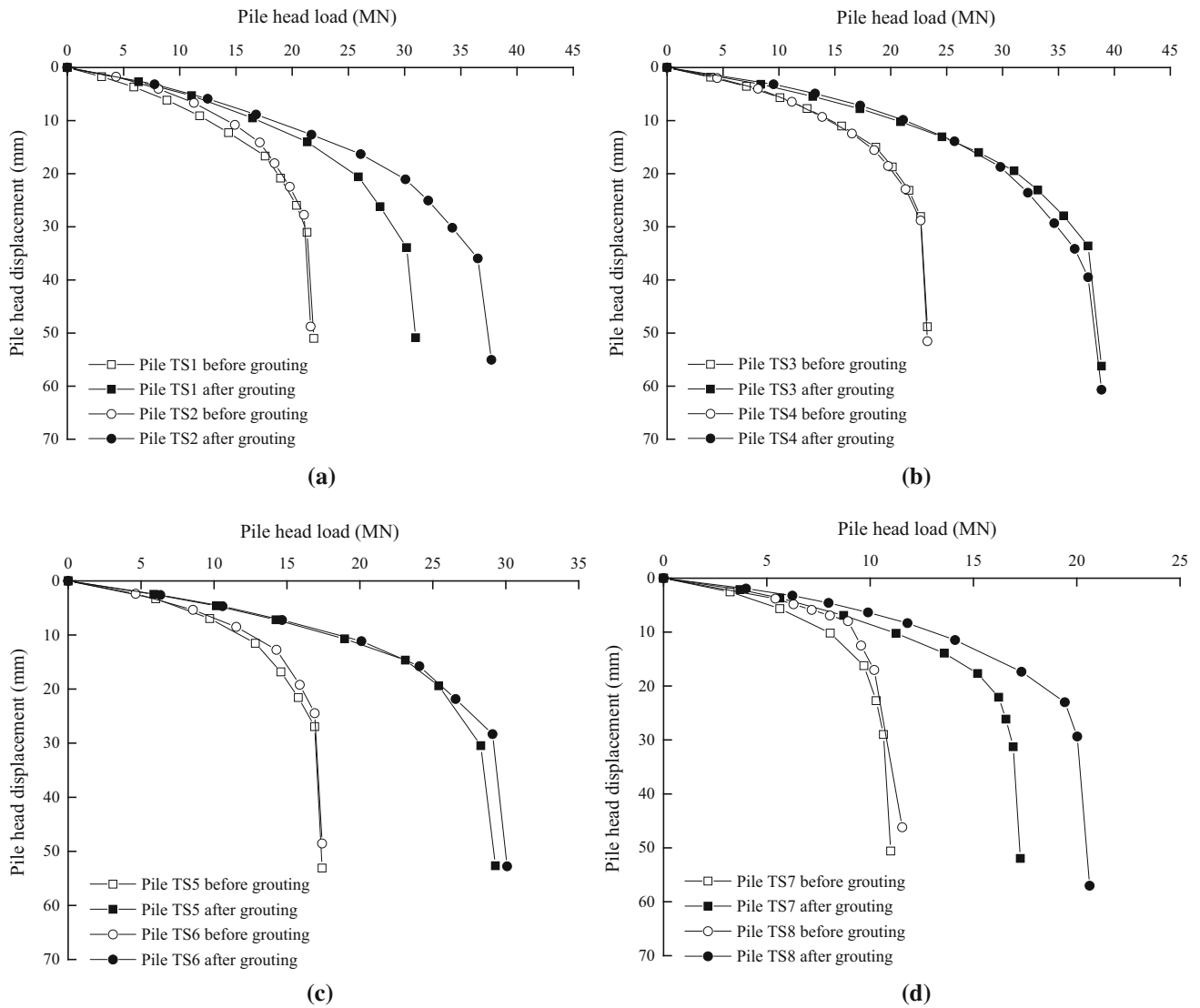


Fig. 8 Equivalent load versus displacement curves of each pile before and after post-grouting: **a** TS1 and TS2; **b** TS3 and TS4; **c** TS5 and TS6; and **d** TS7 and TS8

Table 4 Ultimate bearing capacities, total shaft resistances, base resistances of each pile and their corresponding increased range

Pile no.	Before post-grouting			After post-grouting			$\frac{Q'_{su}-Q_{su}}{Q_{su}}$ (%)	$\frac{Q'_{bu}-Q_{bu}}{Q_{bu}}$ (%)	$\frac{Q'_u-Q_u}{Q_u}$ (%)
	Total shaft resistance Q_{su} (kN)	Mobilized base load Q_{bu} (kN)	Ultimate bearing capacity Q_u (kN)	Total shaft resistance Q'_{su} (kN)	Mobilized base load Q'_{bu} (kN)	Ultimate bearing capacity Q'_u (kN)			
TS1	16,975	4346	21,321	25,777	4401	30,178	51.85	1.27	41.54
TS2	16,803	4243	21,046	26,365	10,148	36,513	56.91	139.17	73.49
TS3	17,878	4798	22,676	26,235	11,413	37,648	46.74	137.87	66.03
TS4	17,897	4779	22,676	26,258	11,390	37,648	46.72	138.33	66.03
TS5	14,385	2520	16,905	21,784	6507	28,291	51.44	158.21	67.35
TS6	14,565	2340	16,905	22,618	6473	29,091	55.29	176.62	72.09
TS7	9370	1275	10,645	14,916	2007	16,923	59.19	57.41	58.98
TS8	9091	1104	10,195	15,353	4670	20,023	68.88	323.01	96.40

7.2 Shaft resistance

The total shaft resistance was gained by subtracting the mobilized base load from the ultimate load capacity, and the pile head displacement was obtained by the equivalent conversion of the results of the bi-directional O-cell test. The relationships between the total shaft resistance and the pile head settlement of each pile before and after post-grouting are given in Fig. 9.

It can be observed from Fig. 9 that the changing trends of the total shaft resistance of each pile before and after post-grouting are almost identical to the pile head displacement but have different values of the total shaft resistance. The total shaft resistance of grouted piles is significantly larger than that of the pile without post-grouting. The grout may have penetrated into the fine sand layer around the pile shaft because of high-pressure

grouting, and the boundary conditions at the pile-soil contact may be improved and increase adhesion of the concrete to the fine sand layer, resulting in high soil strength and stiffness surrounding the pile. The total shaft resistance of the grouted pile is thereby larger than that of the ungrouted pile. In addition, the pressure grout compacts the soil around the pile shaft and increases the horizontal stress at the pile-soil interface, which has a significant and positive impact on the improvement of the shaft resistance.

Figure 10 shows the distribution of the unit shaft resistance along the piles TS1, TS2, TS7, and TS8 before and after post-grouting under the ultimate loading. It can be seen from Fig. 10 that, compared with the test results of the piles TS1, TS2, TS7, and TS8 before post-grouting, the unit shaft resistance of the piles after post-grouting is obviously improved. The increased range of the unit shaft resistance for the combined-grouting piles TS2 and TS8 is

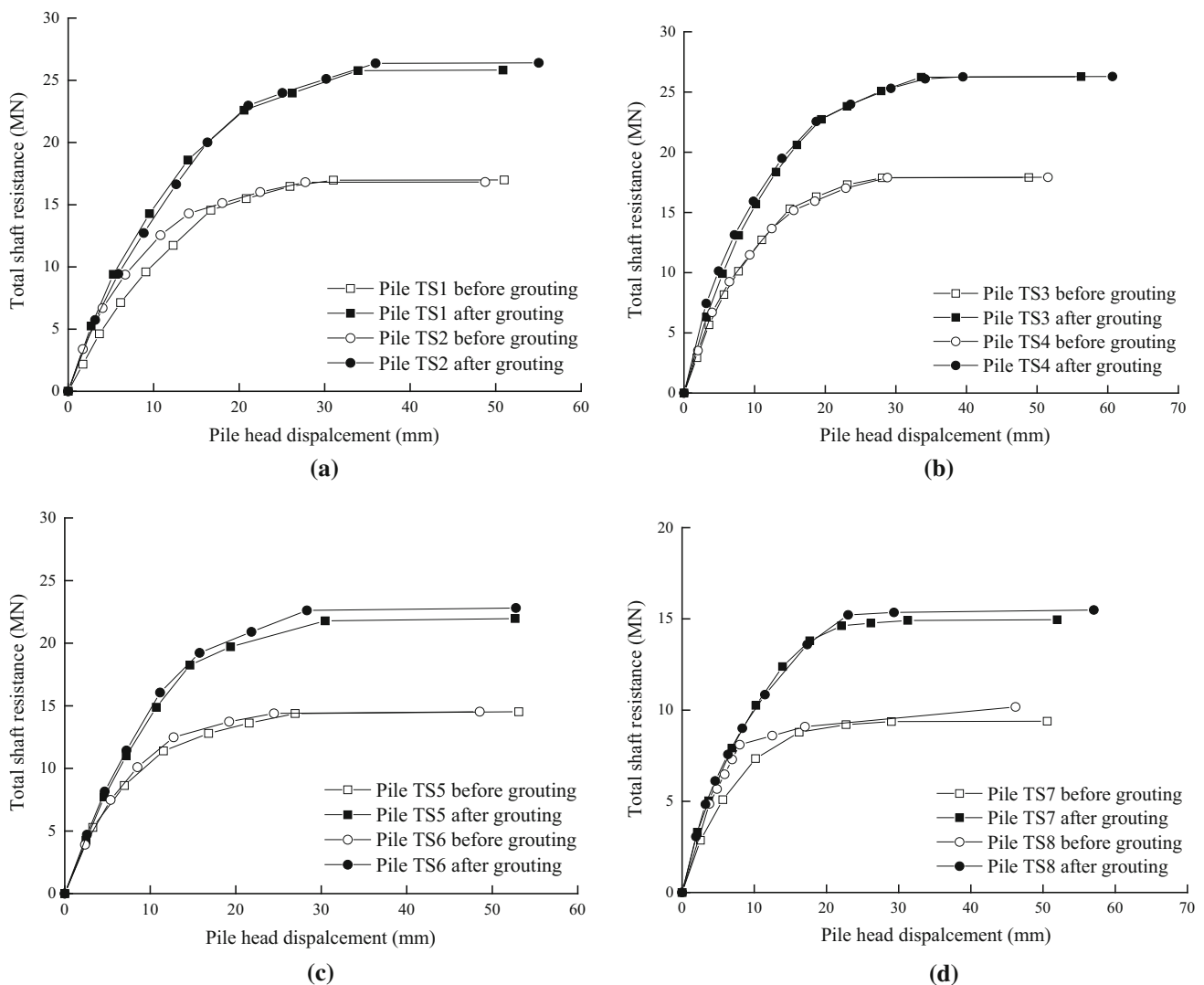


Fig. 9 Total shaft resistance versus pile head displacement curves of each pile before and after post-grouting: **a** TS1 and TS2; **b** TS3 and TS4; **c** TS5 and TS6; and **d** TS7 and TS8

higher than that of the side-grouting piles TS1 and TS7, especially for the unit shaft resistance near the pile tip. It should be noted that the tip grouting for the combined-grouting pile may improve the shaft-soil contact near the pile tip due to migration of the grout along the pile shaft, yielding high soil strength and stiffness surrounding the pile, and the unit shaft resistance is therefore improved. Alternately, the tip grouting can compact and penetrate the fine sand layer at the pile tip and mix with the fine sand layer to effectively strengthen it, making it stronger and stiffer. Therefore, the strengthening effect of the soil improvement at the pile tip on the shaft resistance can enhance the unit shaft resistance.

7.3 Mobilized base resistance

The base resistance for the pile is obtained by subtracting the shaft resistance of the lower pile segment from the lower O-cell load, whereas the base displacement is obtained by subtracting the compression of the lower pile segment from the downward displacement of the lower O-cell load. Therefore, the base resistance-base displacement curves of each pile before and after post-grouting can be obtained, as shown in Fig. 11.

It can be found from Fig. 11 that the base resistance-base displacement curves of the piles before and after post-grouting are similar but have different values of the base resistance. The base displacement after post-grouting is less than that before post-grouting at the same base resistance, which indicates that the end-bearing capacity can be mobilized within a smaller displacement after post-grouting. The pressure grout effectively strengthens the loose sediment at the pile tip and the mudcake around the pile shaft by means of compacting, permeating, and splitting, yielding high strength and stiffness of the soil at the pile

tip. The base resistance of the grouted pile is therefore larger than that of the ungrouted pile. It can also be observed that, compared with the base resistance for the piles TS1 and TS7 before side grouting, the base resistance for the piles TS1 and TS7 after side grouting is increased by 1.27% and 57.41%, respectively, which indicates that side grouting can not only enhance the strength of the soil around the pile shaft but also improve the strength of the soil at the pile tip. It is noted that side grouting effectively solidifies the mudcake around the pile shaft by means of compacting, permeating, filling, and consolidating, whereas the strengthening effect of the surrounding soil improvement on mobilizing the base resistance can enhance the unit base resistance. Additionally, the base resistance for the piles TS2 and TS8 after combined tip-and-side grouting is larger than that of the piles TS2 and TS8 before combined tip-and-side grouting. It also reflects that a more significant effect can be achieved compared with side grouting, and then the tip responses of the combined-grouting pile also have a more significant impact.

Figure 12 shows the relationship between the equivalent pile head load and the mobilized base load for the piles TS1, TS2, TS7, and TS8 before and after post-grouting. It shows that the base load is gradually mobilized with increasing equivalent pile head load. The ratios of the mobilized base load to the equivalent pile head load for the piles before post-grouting are almost identical as the equivalent applied load increases, whereas the mobilized base load sharing ratios of the piles after post-grouting have some discrepancies due to the different types of grouting, i.e., when the piles reach the ultimate load, the mobilized base load sharing ratios of the combined-grouting piles TS2 and TS8 are 22.29% and 23.32%, respectively, and the mobilized base load sharing ratios of the side-grouting piles TS1 and TS7 are 14.58% and 11.86%,

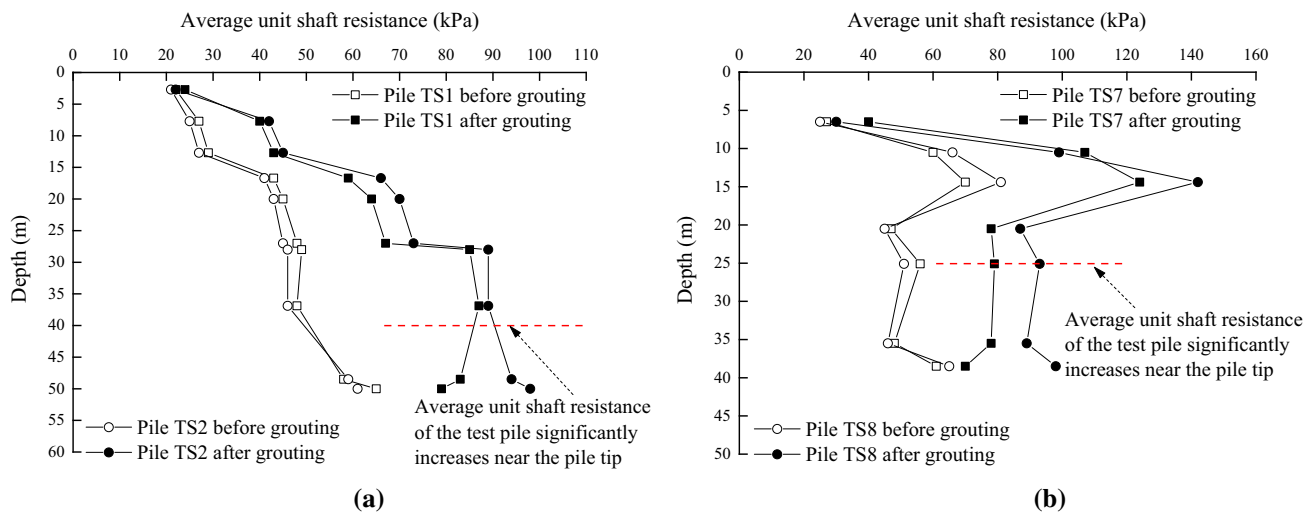


Fig. 10 Average unit shaft resistance of each section for each pile before and after post-grouting: a TS1 and TS2; and b TS7 and TS8

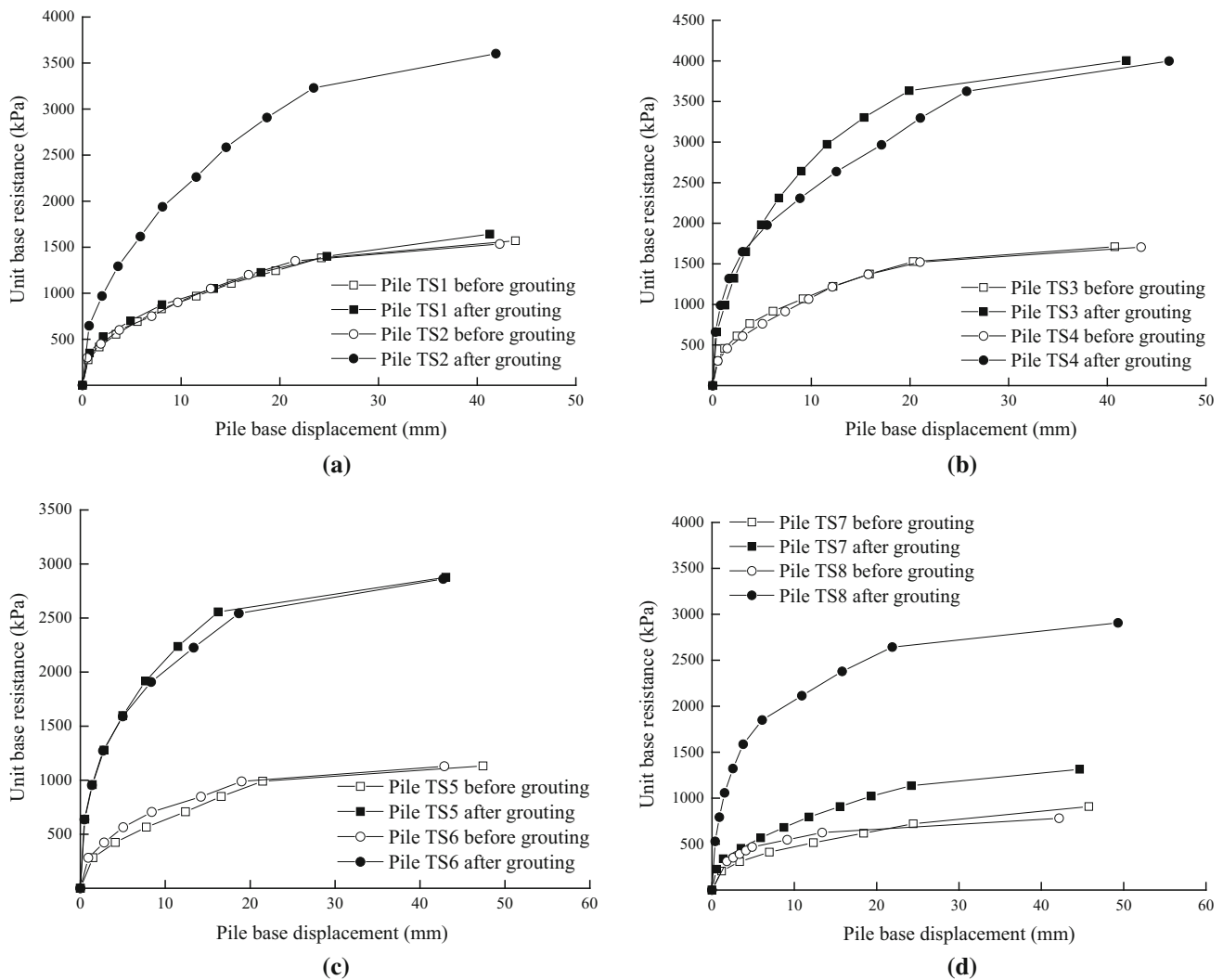


Fig. 11 Pile base resistance versus base displacement curves of each pile before and after post-grouting: **a** TS1 and TS2; **b** TS3 and TS4; **c** TS5 and TS6; and **d** TS7 and TS8

respectively. Therefore, different types of grouting may lead to different bearing performances of the pile. It can also be observed that the base resistance of the combined-grouting pile is mobilized before the application of vertical load because of the preloading effect of soil beneath the pile tip arising from the tip grouting. Thus, the strain incompatibility between the base resistance and the shaft resistance of the combined-grouting pile is improved.

8 Application of the EWCT technique in detecting post-grouting effects

8.1 Principle of the EWCT technique

Electromagnetic Wave Computerized Tomography (EWCT), as a modern nondestructive testing technique to

identify and classify the characteristics of geological structures, has been employed in a variety of application fields. The EWCT technique is a geophysical prospecting method in which electromagnetic waves are sent into a borehole and received in another borehole, and the two-dimensional distribution of the absorption coefficient of the underground medium is studied by using the inversion algorithm according to the data obtained from different depths between the boreholes [4, 8, 12, 30]. The theory and practice have proved [12, 14, 30] that the transmission of an electromagnetic wave in the underground media is principally influenced by the electrical conductivity, dielectric permittivity and frequency of the electromagnetic wave, and there is thereby some discrepancy in the absorption of the electromagnetic wave in the underground media. Therefore, these differences can be used to infer the position and shape of underground structures via the EWCT technique.

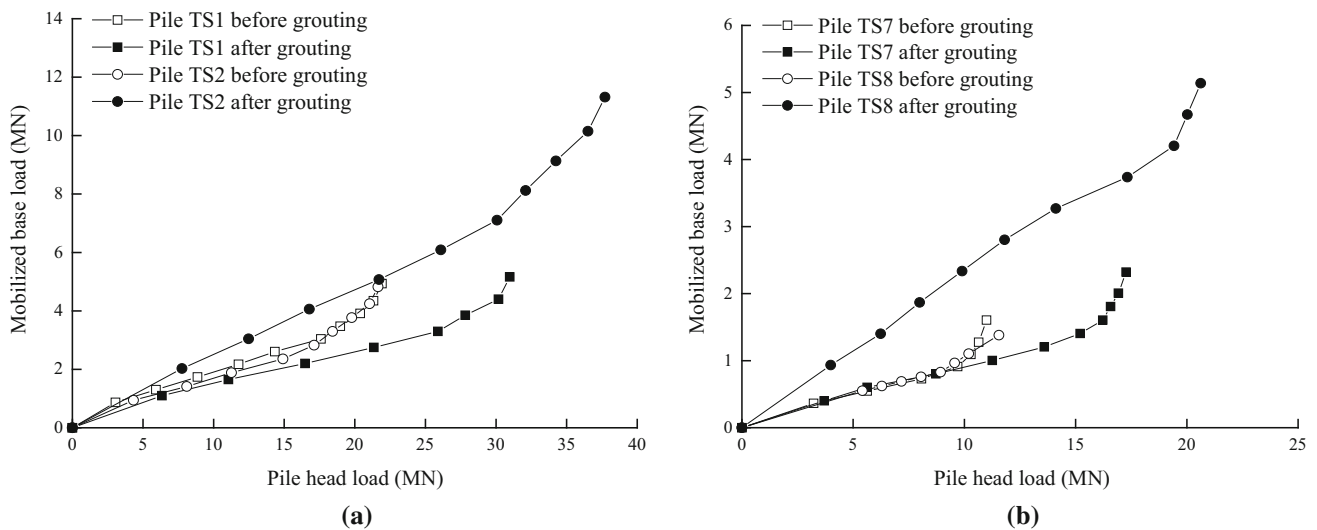


Fig. 12 Equivalent pile head load versus mobilized base load curves of each pile before and after post-grouting: **a** TS1 and TS2; and **b** TS7 and TS8

The injected cement grout mixes with the undisturbed soil particles by means of filling, permeating, compacting, and splitting and is condensed into a cement–soil material with high strength and stable chemical performance. There is thereby some discrepancy in the absorption coefficient between the undisturbed soil and the cement stabilized soil, and the grouting effect of the grouted pile is studied on the basis of different absorption coefficients. Consequently, the EWCT technique can be adopted to assess the reinforcement effect of post-grouting on the pile foundation.

8.2 Test details, test method, and test procedure

To explore the application of the EWCT technique in the Shishou Yangtze River Highway Bridge project, the test piles TS3 and TS4 were selected as the EWCT test object. The EWCT tests were carried out 38 days after post-grouting. In this test, a crosshole electromagnetic wave method was applied to a PVC pipe with a diameter of 60 mm embedded in the boreholes. Both the test piles have four boreholes drilled around the pile side as the transmission borehole and the receiver borehole, respectively, and the vertical distances between the four boreholes and the pile side are 0.5, 0.5, 2.0, and 4.0 m, respectively. To analyze the test results of the EWCT for the piles TS3 and TS4 after post-grouting, a fictitious pile is set up as a comparison. Similarly, the fictitious pile has four boreholes drilled around the pile side. Each pile, which forms a crosshole plane between the transmitter in one borehole and the receiver in another, is a total of six crosshole planes, i.e., separate data sets for the pile TS3 are acquired along six sections between boreholes B and A, B and C, A and D, C and D, B and D, and C and A. Note that the

coring hole is taken as borehole J to facilitate the test. The detailed arrangement of the EWCT test holes for each pile is shown in Fig. 13.

In practice, a transmitter antenna set to a well-defined frequency is first placed in the transmission borehole and fixed at a given depth, and then a receiver antenna set to the same frequency is lowered to the receiver borehole, moves upwards or downwards at intervals of 1 m along the receiver borehole, and receives signals once at intervals; thus, a series of data can be acquired as a scan. Subsequently, the transmitter antenna is moved upwards or downwards at intervals of 1 m, and another scan can be conducted until the entire length of the two boreholes is scanned. In the specific test, the antennae frequencies of 12, 18, and 24 MHz are tested separately to ensure that the antennae frequency of the appropriate electromagnetic wave is obtained. Therefore, the data analysis phase is interpreted by electromagnetic wave data with the antennae frequency of 12 MHz because of the influence of the spacing of boreholes on the resolution.

The EWCT technique in detecting post-grouting effects includes the following steps: (1) ensure that the boreholes are first smooth and complete the preparation before the test; (2) a transmitter antenna and a receiver antenna are placed in the boreholes, and the transmitter antenna and receiver antenna are connected to the host system through the electric cable to control and debug the instrument parameters; (3) the transmitter antenna or the receiver antenna is moved upwards or downwards at intervals of 1 m using the fixed-point transmitting method, and the related data is acquired to complete the scanning of the entire length of the two boreholes by the automatic monitoring system; (4) check whether the data is normal,

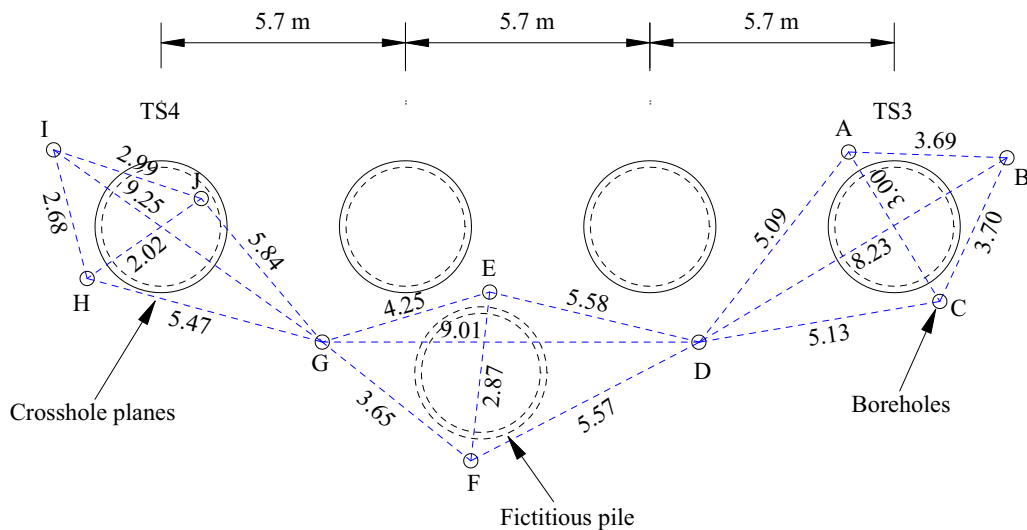


Fig. 13 The arrangement of the EWCT test holes for each pile (unit: m)

and re-test for any special case; and (5) the data is then interpreted using the related treatment software, and an image of the underground medium between the two boreholes is obtained in the distribution form of the scanning of the entire length. Following the abovementioned procedure, the grouting effect of the cement grout on the soil between the boreholes can be obtained, and the grouting effect of each crosshole plane can be obtained by repeating the abovementioned steps, thereby realizing the evaluation of the grouting effect of post-grouting on the pile foundation.

8.3 Analysis of the EWCT test results

Data acquired with the transmitter boreholes and receiver boreholes in this EWCT test was analyzed and interpreted. The apparent absorption coefficient β of the electromagnetic wave in the underground media was first obtained using the algebraic reconstruction method, and then the inversion image of the apparent absorption coefficient of each crosshole plane was drawn by the related software. The inversion images of the apparent absorption coefficient of each crosshole plane for each pile are shown in Figs. 14, 15, and 16.

Figure 14 shows the inversion image of the apparent absorption coefficient of each crosshole plane for the fictitious pile. It can be observed that there is some discrepancy in the apparent absorption coefficient between partial crosshole planes, which may be affected by the spacing of boreholes, the squeezing effect of adjacent piles, pressure grout that penetrates and compacts the surrounding soil, etc. The crosshole plane between boreholes G and F can be divided into three parts from top to bottom, and there is a clear stratification boundary of the

apparent absorption coefficient at depths approximately 17 and 38 m, that is, the properties of the soil have changed, which is more consistent with the geological prospecting data.

Figure 15 shows the inversion image of the apparent absorption coefficient of each crosshole plane for the test pile TS3. It can be found that the inversion images of the apparent absorption coefficient of the crosshole planes BA and BC are similar in the overall characteristics, and the inversion images of the apparent absorption coefficient of the crosshole planes AD and CD are also similar in the overall characteristics. Compared with the inversion image of apparent absorption coefficient of each crosshole plane for the fictitious pile, it is inferred that the apparent absorption coefficient β of the cement grout reinforcement zone should be approximately 0.8 dB/m. The β value of the crosshole planes BA and BC is too large because of the distance between the boreholes, whereas the β value is abnormally small at depths between 14 and 16 m, and the β value near boreholes A and C is smaller. It is thus deduced that the soil in this depth range is affected by the reinforcement of the cement grout. Meantime, the inversion images of the apparent absorption coefficient of the crosshole planes AD and CD also show the impact of the cement grout on the soil in this depth range; this indicates that the grouting at the pile side 15 m below the ground surface is more uniform, and the cement grout is horizontally distributed in the range of 2–3 m around the pile. Additionally, an anomalous layer appears at depths between 31 and 33 m by observing the inversion image of each crosshole plane, and it can thus be deduced that the layer is a thin silty soil combined with the geological prospecting data. The crosshole planes BD near the direction of the fictitious pile formed a one-way expansion,

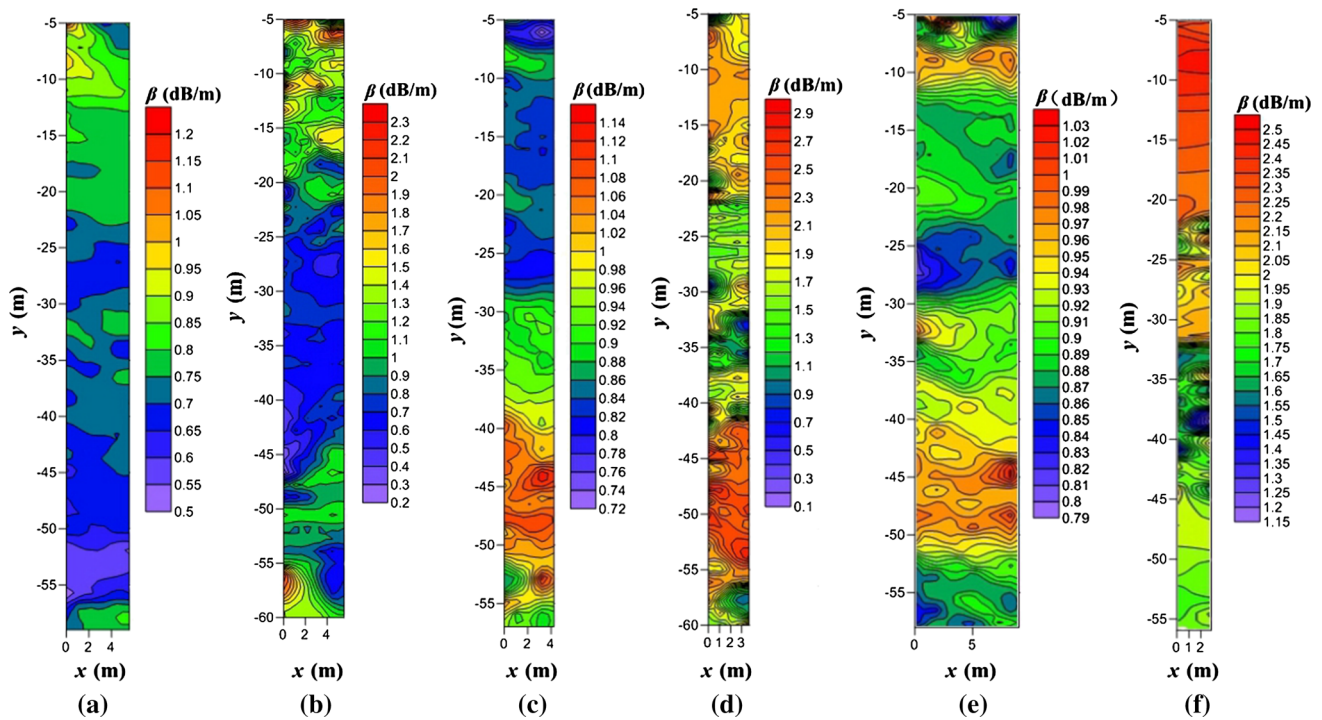


Fig. 14 The inversion image of the apparent absorption coefficient of each crosshole plane for the fictitious pile: **a** E–D; **b** D–F; **c** E–G; **d** G–F; **e** D–G; and **f** E–F

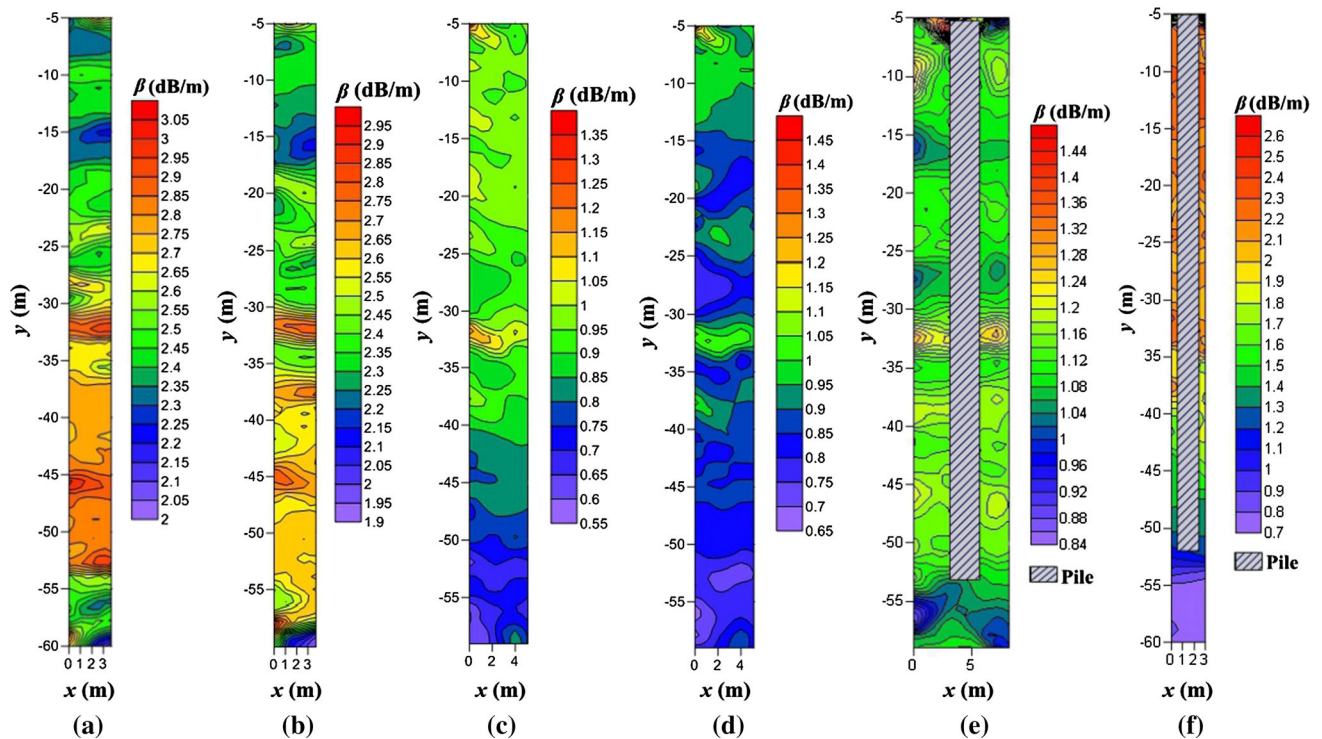


Fig. 15 The inversion image of the apparent absorption coefficient of each crosshole plane for test pile TS3: **a** B–A; **b** B–C; **c** A–D; **d** C–D; **e** B–D; and **f** C–A

and the inversion images of the fictitious pile can be used to determine the horizontal penetration of the cement grout in the range of 2–3 m.

It can also be observed from Fig. 15 that the β value of the crosshole planes AD and CD below 40 m decreases from 0.8 to 0.55, whereas the β value of the crosshole

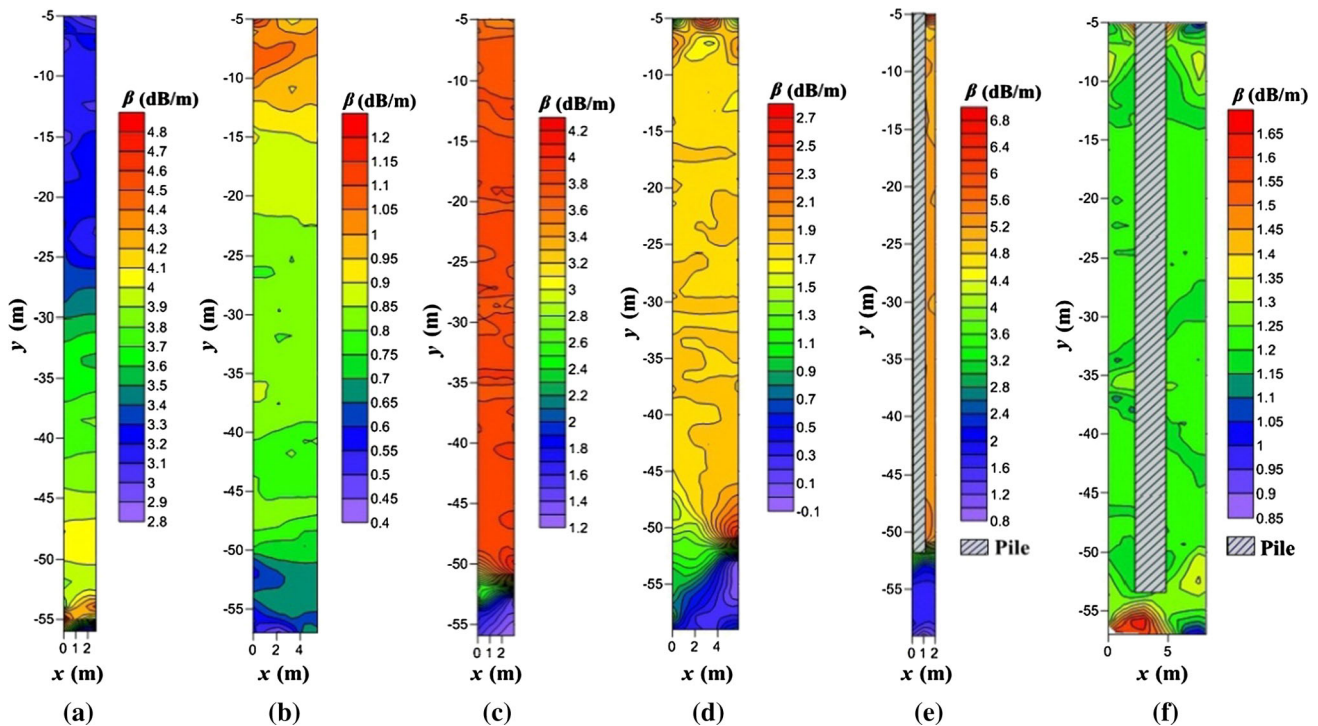


Fig. 16 The inversion image of the apparent absorption coefficient of each crosshole plane for test pile TS4: **a** I–H; **b** G–H; **c** I–J; **d** G–J; **e** H–J; and **f** I–G

planes BA and BC does not reflect this phenomenon. This indicates that the grout migrates along the shaft side near the direction of the fictitious pile due to tip grouting and forms an uneven enlarged head. In addition, the inversion image of the crosshole plane BD shows that the reinforcement effect of the pile tip is significantly obvious, and the maximum reinforcement depth can reach 4–5 m below the pile tip.

Figure 16 shows the inversion image of the apparent absorption coefficient of each crosshole plane for the test pile TS4. The coring hole is taken as borehole J, and steel casings in the coring hole have a greater impact on the electromagnetic waves. Hence, the resolution of the inversion image of the crosshole planes IJ, GJ, and HJ in the pile length range is relatively poor. Alternately, the resolution of the inversion image of the crosshole planes IH and IG is unsatisfactory due to the distance between the transmission borehole and the receiver borehole. Therefore, the effect of the pile tip grouting is only analyzed for the test pile TS4.

It can be seen from the crosshole planes GH, IJ, GJ, and HJ that the β value appears in an anomalous region approximately 51 m below the ground surface, which indicates that the soil in this depth is affected by the reinforcement of cement grout at the pile tip. The crosshole planes IJ and GJ at the pile tip J exhibit false contours and spread gradually toward the direction of I and G. This shows

that the phenomenon of false contours may be affected by the excessive deposition of the grout at the pile tip and the vertical grout due to the tip grouting being unevenly distributed. In addition, the inversion image of the crosshole planes HJ shows that the cement grout penetrates and spreads toward the soil below the pile tip; it can be deduced that the maximum reinforcement depth can reach 5–7 m below the pile tip, and the cement grout is horizontally distributed in the range of 3–4 m around the pile.

In the analysis of the EWCT test results of the above-mentioned single pile, the apparent absorption coefficient β reflected by the inversion image of partial crosshole planes is quite different due to the influence of the spacing of boreholes and the pile shaft. Therefore, the crosshole planes CD, DG, and GH with good test results are analyzed uniformly, and the inversion image of the apparent absorption coefficient of the entire region can be obtained, as shown in Fig. 17. It shows that the fictitious pile at depths between 13 and 30 m is affected by the penetration of the cement grout, and the cement grout of side-grouting for the test piles TS3 and TS4 is connected in the transverse direction. It is thus deduced that this may be affected by the squeezing effect of the adjacent piles, and the injected cement grout infiltrates into a small confining pressure in the direction of the fictitious pile.

Based on the above analysis, the influencing factors of the EWCT detection effect can be summarized as follows:

(1) the β value of the apparent absorption coefficient exhibits easily abnormal phenomena due to the close distance between the transmission borehole and the receiver borehole, resulting in the relatively poor resolution of the inversion image; (2) the influence of reinforced concrete piles on the detection of electromagnetic waves, the crosshole plane across the pile shaft, and the smaller spacing of boreholes prevent detection of the effect of side-grouting; and (3) steel casings have a greater impact on the electromagnetic waves, which easily results in the lower resolution of the inversion image of the crosshole planes.

9 In situ standard penetration test

In the post-grouting process of the pile foundation, the injected cement grout mixes with the soil at the pile tip and side into a cement–soil material, yielding a greater difference between the properties and status of the cement stabilized soil and the original soil, and thus the blowcounts of penetration to the same depth may be different. Therefore, the in situ standard penetration test can be applied to evaluate the post-grouting effect of the pile foundation by the variation of SPT blowcounts (N) before and after post-grouting. The SPT in this test is only studied for the test piles TS1, TS3, and TS4. The holes A and B at the pile side are arranged symmetrically on both sides of each test pile, and the spacing between the side hole and the pile side is 20 cm. Figure 18 shows the arrangement of the SPT holes for each pile. Each pile was subjected to the SPT test 35 days after post-grouting and compared with the SPT N value of a geological survey of the same location for

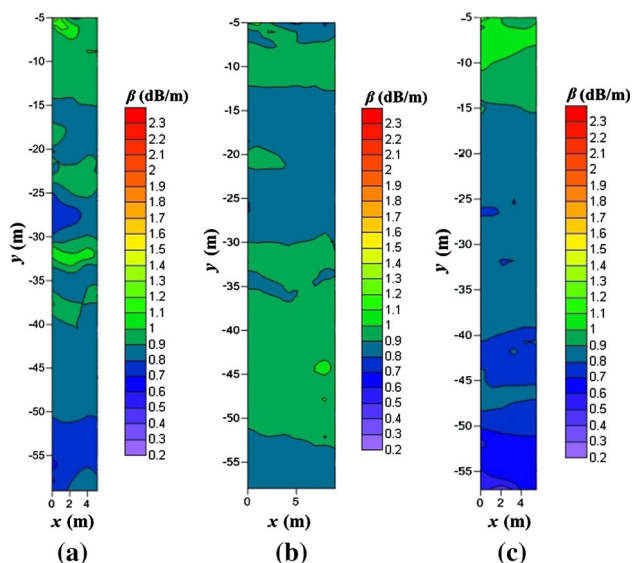


Fig. 17 The inversion image of the apparent absorption coefficient of the entire region: **a** C–D; **b** D–G; and **c** G–H

each pile. Comparisons of SPT N value for the piles before and after post-grouting are shown in Fig. 19.

It can be observed from Fig. 19 that the SPT N value after post-grouting for the pile TS1 above 18 m in depth is slightly less than that before post-grouting. It is inferred that the cement grout distribution of the pile side-grouting is non-uniform, and thus the test results have a certain limitation. The SPT N value of the soil at the pile side after combined grouting is generally improved. This indicates that the cement grout is filled with the defects of the pile-soil surface to enhance the strength and stiffness of the soil at the pile side, and the SPT N value of the soil at the pile side after post-grouting is thereby larger than that before post-grouting.

Figure 20 shows the relationship between unit shaft resistance and SPT N value before and after post-grouting. For clarity, the ratios of the unit shaft resistance are used for analysis. In Fig. 20, it is shown that the ratios of the unit shaft resistance to the SPT N value before and after post-grouting gradually decreases with an increasing SPT N value and tends to be stable. It is also obvious that compared with those before post-grouting, the ratios of the unit shaft resistance to the SPT N value after post-grouting are much larger for any given SPT N value. It is further indicated that the injected cement grout is filled with the defects of the pile-soil interface to improve the boundary conditions at the pile-soil contact, and enhance the strength and stiffness of the soil around the pile shaft, thereby enhancing the unit shaft resistance.

10 Discussion

In the present study, we investigated the bearing behavior of cast-in-place bored piles with different types of post-grouting. The test results demonstrate that the bearing performance of the combined-grouting pile is better than that of the side-grouting pile. Wan and Qiu [41] reported that post-grouting at the pile side strengthens the surrounding soil by means of compacting and permeating, the

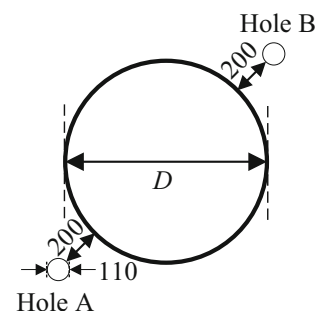


Fig. 18 The arrangement of the SPT holes for test piles TS1, TS3, and TS4 (unit: mm)

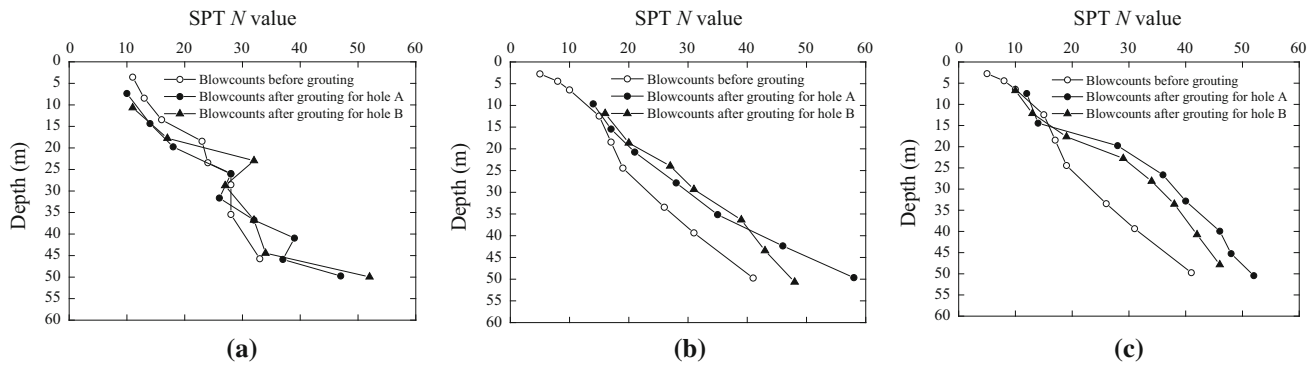


Fig. 19 Comparison of the SPT N values for each pile before and after post-grouting: **a** TS1; **b** TS3; and **c** TS4

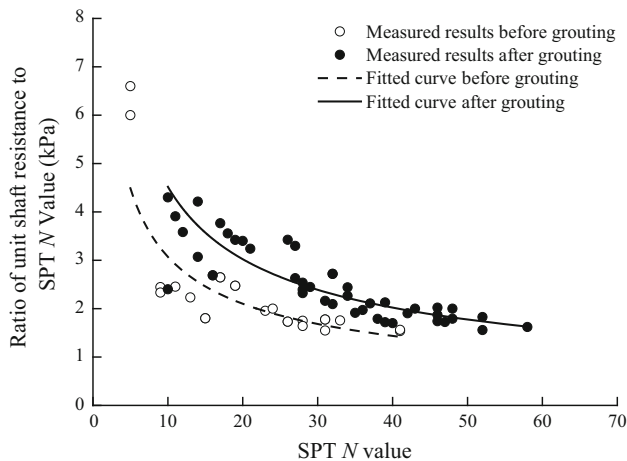


Fig. 20 Relationship between unit the shaft resistance and SPT N value before and after post-grouting

strength and stiffness of the grouting soil are higher than that of the non-grouting soil, and the horizontal bearing capacity of bored piles can be improved significantly. Therefore, when large-diameter bored piles are subjected to large horizontal loads, post-grouting at the pile side can be used to increase their horizontal bearing capacity; if large-diameter bored piles are subjected to a combination of vertical and horizontal loads, combined tip-and-side grouting can be used to significantly improve its bearing performance.

The strengthening effect of the stiff soil at the pile tip on the shaft resistance was discussed by Zhang et al. [45]. In this study, we not only observed the strengthening effect of the soil improvement at the pile tip due to tip grouting on the shaft resistance but also found that the base resistance can be increased by the surrounding soil improvement due to side grouting. Consequently, by revealing the mechanism of the strengthening interaction between the shaft and base resistance, the potential bearing capacity of post-grouting piles can be mobilized to achieve the optimal design of pile foundations and reasonably correct the calculation method of bearing capacity of pile foundations.

In this test, the static load test and the standard penetration test are only suitable for the representative test piles as the detection methods of grouting effect. However, these two methods have great limitations for evaluating multi-pile or pile group foundations. The results of the EWTC test indicate that the method can be employed to detect the grouting effect of post-grouting piles, and it can be applied to practical mass production piles. Indeed, the EWCT technique has been widely used in engineering geological exploration, quality inspection of pile foundations and the detection of karst roadbed grouting because of its high accuracy and intuitive analytical results and the fact that it is unaffected by the obstruction of obstacles on the ground and the overburden thickness [16, 30, 42]. Therefore, it is further shown that it is completely feasible to detect the grouting effect of the pile foundation by using the EWCT technique. The main purpose of this work is to reveal the influence of different grouting types on the bearing characteristics of large-diameter bored piles and to use the EWCT technique to realize the evaluation of the grouting effect for post-grouting piles. The research results have significant guidance for the design and effect detection of post-grouting piles.

11 Conclusion

This paper presents the results of field tests performed on six combined side-and-tip grouting piles and two side-grouting piles constructed in an extra-thick fine sand layer in the region of Shishou, China. The reinforcement effect of post-grouting was evaluated using the EWCT technique and standard penetration test. The following conclusions can be drawn on the basis of the test results and analyses.

1. The ultimate bearing capacity of side-grouting piles in the extra-thick fine sand layer is increased by 41.54–58.98%, and the ultimate bearing capacity of combined-grouting piles is increased by

- 66.03–96.40%. The test results show that the grouted piles provide larger load-bearing capacity than ungrouted piles under the same conditions, and the combined-grouting piles provide also greater load-bearing capacity than side-grouting piles.
2. Post-grouting at the pile side effectively improves the boundary conditions between the pile shaft and the soil and enhances the soil strength and stiffness surrounding the pile. Therefore, the total shaft resistances after post-grouting are 46.72–68.88% higher than those before post-grouting and have significant effects on the load transfer characteristics of the pile.
 3. The mobilized base resistance of grouted piles is larger than that of the piles without grouting at the same base displacement, and the end-bearing capacity can be developed within smaller displacement after post-grouting. In addition, the increased ranges of the base resistance for the combined-grouting piles and side-grouting piles are 1.27–57.41% and 137.87–323.01%, respectively, which indicates that the effect of the combined-grouting piles is obviously better than that of the side-grouting piles, and the tip responses of combined-grouting piles also have a more significant impact.
 4. The increased range of the unit shaft resistance for the combined-grouting piles TS2 and TS8 is larger than that of the side-grouting piles TS1 and TS7, especially for the unit shaft resistance near the pile tip; this reflects that the strengthening effect of the soil improvement at the pile tip on the shaft resistance can enhance the unit shaft resistance. The base resistances of the side-grouting piles TS1 and TS7 are 1.27% and 57.41% higher than those of ungrouted piles, respectively, which indicates that the strengthening effect of the surrounding soil improvement on mobilizing the base resistance can increase the unit base resistance. Consequently, the test results show the strengthening interaction between the shaft and base resistance.
 5. The EWCT test shows that it is feasible to detect the grouting effect by using the EWCT technique. The distribution pattern of the pile, injected grout and geotechnical interface can be observed by the inversion image of the apparent absorption coefficient of each crosshole plane, and the diffusion range of the cement grout in the soil at the pile tip and side can be deduced to evaluate the grouting effect of the grouted pile.
 6. The EWCT detection effect is affected by the distance between the transmission borehole and the receiver borehole, reinforced concrete piles, and steel casings, resulting in the relatively poor resolution of the inversion image. Therefore, the conclusions obtained

in this test have good application value and can provide the basis for the effect detection of future post-grouting piles.

7. The standard penetration test shows that the SPT N value of the soil at the pile side after post-grouting is generally increased, and the shaft resistance of the fine sand layer before and after post-grouting increases linearly with the increase in the SPT N value; the unit shaft resistance after post-grouting is thus larger than that before post-grouting. It is therefore further indicated that post-grouting at the pile side can improve the shaft resistance by enhancing the strength and stiffness of the soil around the pile shaft.

Acknowledgements The authors are very grateful to the reviewers for their helpful comments and constructive suggestions in improving this paper.

Funding This work was supported by the National Natural Science Foundation of China (Nos. 51478109; 51678145), and the Priority Academic Program Development of Jiangsu Higher Education Institutions (No. 1105007002).

References

1. Bolognesi AJL, Moretto O (1973) Stage grouting preloading of large piles on sand. In: Proceedings of 8th ICSME, Moscow, vol 2, no 1, pp 19–25
2. Bruce DA (1986) Enhancing the performance of large diameter piles by grouting. *Ground Eng* 19(4):9–15
3. Byrne GP, Strydom JH, Du Preez W (1998) The performance of piled foundations supporting a large hotel on estuarine deposits in Durban. In: International conference and exhibition on piling and deep foundations, pp 1–1.21
4. Cote P, Degauque P, Lagabrielle R, Levent N (1995) Detection of underground cavities with monofrequency electromagnetic tomography between boreholes in the frequency range 100 MHz to 1 GHz. *Geophys Prospect* 43(8):1083–1107
5. Dai GL, Gong WM, Xue G, Tong XD (2006) Effect examination for a base post-grouted overlength drilling pile. *Rock Soil Mech* 27(5):849–852 (in Chinese)
6. Dai G, Gong W, Zhao X, Zhou X (2010) Static testing of pile-base post-grouting piles of the Suramadu bridge. *Geotech Test J* 34(1):34–49
7. Dapp SD, Mullins G (2002) Pressure grouting drilled shaft tips: full-scale research investigation for silty and shelly sands. In: Deep foundations: an international perspective on theory, design, construction, and performance, pp 335–350
8. Dines KA, Lytle RJ (1979) Computerized geophysical tomography. *Proc IEEE* 67(7):1065–1073
9. Duan X, Kulhawy FH (2009) Tip post-grouting of slurry-drilled shafts in soil: Chinese experiences. In: Contemporary topics in deep foundations, ASCE, pp 47–54
10. Fu X, Zhou Z (2003) Study on bearing capacity of bored cast-in situ piles by post pressure grouting. In: Grouting and ground treatment, pp 707–715
11. Gouvenot D, Gabaix JC (1975) A new foundation technique using piles sealed by cement grout under high pressure. In: Offshore technology conference, Texas, USA, pp 645–656

12. Gu H, Cai C, Wang Y (2006) Investigation of fractures using seismic computerized crosshole tomography. *J Environ Eng Geophys* 11(2):143–150
13. Ho CE (2003) Base grouted bored pile on weak granite. In: *Grouting and ground treatment*, pp 716–727
14. Hu Y, Xie Q, Zhao W, Zheng LN (2013) Electromagnetic wave CT detection standard of karst roadbed grouting. *J Southwest Jiaotong Univ* 48(3):441–447 (in Chinese)
15. Joer HA, Randolph MF, Gunasena U (1998) Experimental modeling of the shaft capacity of grouted driven piles. *Geotech Test J* 21(3):159–168
16. Li CM, Wang LS, Zhong K (2003) Application of electromagnetic wave computerized tomography to testing quality of pile. *Geol J China Univ* 9(3):467–473 (in Chinese)
17. Lin SS, Lin T, Chang LT (2000) A case study for drilled shafts base mud treatment. In: *New technological and design developments in deep foundations*, pp 46–58
18. Littlechild BD, Plumbridge GD, Free MW (1998) Shaft grouted piles in sand and clay in Bangkok. In: *Proceedings of the 7th international conference and exhibition on piling and deep foundations*, DFI, Vienna, pp 171–178
19. Littlechild BD, Plumbridge GD, Hill SJ, Lee SC (2000) Shaft grouting of deep foundations in Hong Kong. In: *New technological and design developments in deep foundations*, pp 33–45
20. Lizzi F, Viggiani C, Vinale F (1983) Some experience with pre-loading cells at the base of large diameter bored piles. In: *Proceedings of the 7th Asian regional conference on soil mechanics and foundation engineering*, Haifa, Israel, pp 265–270
21. Lui JYH, Cheung SPY, Chan AKC (1993) Pressure grouted minipiles for a 12-storey residential building at the Mid-levels Scheduled Area in Hong Kong. In: *Proceedings of the international conference on soft clay engineering*, pp 419–424
22. Majano RE, O'Neill MW, Hassan KM (1994) Perimeter load transfer in model drilled shafts formed under slurry. *J Geotech Eng* 120(12):2136–2154
23. Mullins G, Dapp S, Frederick E, Wanger V (2001) Post grouting drilled shaft tips: phase I. Research report University of South Florida, Tampa, USA, pp 127–156
24. Mullins G, Dapp S D, Lai P (2000) Pressure-grouting drilled shaft tips in sand. In: *New technological and design developments in deep foundations*, pp 1–17
25. O'Neill MW, Reese LC (1976) Behavior of axially loaded drilled shafts in clay-shales. Center for Highway Research, The University of Texas at Austin, Austin
26. Safaqa O, Bittner R, Zhang X (2007) Post-grouting of drilled shaft tips on the Sutong Bridge: a case history. In: *Contemporary issues in deep foundations*, pp 1–10
27. Sliwinski ZJ, Fleming WGK (1984) The integrity and performance of bored piles. In: *Piling and ground treatment*. Thomas Telford Publishing, pp 211–223
28. Stocker MF (1983) The influence of post grouting on the load bearing capacity of bored piles. In: *Proceedings of the 8th European conference on soil mechanics and foundation engineering*, Balkema, Helsinki, pp 167–170
29. Sze JWC, Chan KM (2012) Application of shaft grouting technique in deep foundations-Hong Kong experience. In: *Grouting and deep mixing*, pp 1085–1094
30. Tan H, Huang J, Qi S (2012) Application of cross-hole radar tomograph in karst Area. *Environ Earth Sci* 66(1):355–362
31. Thasnanipan N, Aye ZZ, Submaneevong C (2004) Effectiveness of Toe-grouting for deep-seated bored piles in Bangkok Subsoil. In: *GeoSupport 2004: drilled shafts, micropiling, deep mixing, remedial methods, and specialty foundation systems*, pp 561–572
32. The Professional Standards Compilation Group of People's Republic of China (2008) Technical code for building pile foundation. JGJ94-2008. China Architecture and Building Press, Beijing (in Chinese)
33. The Professional Standards Compilation Group of People's Republic of China (2007) Code for design of ground base and foundation of highway bridges and culverts. JTJD63-2007. China Communications Press, Beijing (in Chinese)
34. The Professional Standards Compilation Group of People's Republic of China (2017) Technical specification for static loading test of self-balanced method of building foundation piles. JGJ/T 403-2017. China Architecture and Building Press, Beijing (in Chinese)
35. Thiyyakkandi S, McVay M, Bloomquist D, Lai P (2013) Measured and predicted response of a new jetted and grouted precast pile with membranes in cohesionless soils. *J Geotech Geoenviron Eng* 139(8):1334–1345
36. Thiyyakkandi S, McVay M, Bloomquist D, Lai P (2014) Experimental study, numerical modeling of and axial prediction approach to base grouted drilled shafts in cohesionless soils. *Acta Geotech* 9(3):439–454
37. Thiyyakkandi S, McVay M, Lai P (2014) Experimental group behavior of grouted deep foundations. *Geotech Test J* 37(4):621–638
38. Wan Z, Dai G (2017) Experiences with tip post grouted drilled shafts in China. In: *International congress and exhibition sustainable civil infrastructures, GeoMEast 2017*. Sharm el Sheikh, pp 330–343
39. Wan Z, Dai G, Gong W (2017) Post-grouting of drilled shaft tips in coral-reef limestone formations: a case study. In: *Proceedings of the 27th international ocean and polar engineering conference*, San Francisco, USA, pp 719–724
40. Wan Z, Dai G, Gong W (2018) Full-scale load testing of two large diameter drilled shafts in coral-reef limestone formations. *Bull Eng Geol Environ* 77(3):1127–1143
41. Wan Z, Qiu RD (2015) Horizontal static load test research for pile lateral friction and tip resistance of grouting technique. *Chin J Rock Mech Eng* 34(Supp1):3588–3596 (in Chinese)
42. Yue CW, Wang ZW, Xu JY (2008) The application of the electromagnetic tomography technique to engineering geology. *Geophys Geochem Explor* 32(2):216–219 (in Chinese)
43. Zhang Q, Li SC, Li LP (2014) Field study on the behavior of destructive and non-destructive piles under compression. *Mar Georesour Geotechnol* 32(1):18–37
44. Zhang ZM, Yu J, Zhang GX, Zhou XM (2009) Test study on the characteristics of mudcakes and in situ soils around bored piles. *Can Geotech J* 46(3):241–255
45. Zhang QQ, Zhang ZM, Li SC (2013) Investigation into skin friction of bored pile including influence of soil strength at pile base. *Mar Georesour Geotechnol* 31(1):1–16
46. Zhou JJ, Gong XN, Wang KH, Zhang RH, Yan JJ (2017) Testing and modeling the behavior of pre-bored grouting planted piles under compression and tension. *Acta Geotech* 12(9):1061–1075
47. Zhou JJ, Gong XN, Wang KH, Zhang RH (2018) Shaft capacity of the pre-bored grouted planted pile in dense sand. *Acta Geotech* 1:1–13